

University of Windsor

## Scholarship at UWindor

---

Electronic Theses and Dissertations

Theses, Dissertations, and Major Papers

---

1-1-2007

### Comparative study of joint stiffness calculations using the finite element analysis.

Negar Rasti  
*University of Windsor*

Follow this and additional works at: <https://scholar.uwindsor.ca/etd>

---

#### Recommended Citation

Rasti, Negar, "Comparative study of joint stiffness calculations using the finite element analysis." (2007). *Electronic Theses and Dissertations*. 7031.  
<https://scholar.uwindsor.ca/etd/7031>

This online database contains the full-text of PhD dissertations and Masters' theses of University of Windsor students from 1954 forward. These documents are made available for personal study and research purposes only, in accordance with the Canadian Copyright Act and the Creative Commons license—CC BY-NC-ND (Attribution, Non-Commercial, No Derivative Works). Under this license, works must always be attributed to the copyright holder (original author), cannot be used for any commercial purposes, and may not be altered. Any other use would require the permission of the copyright holder. Students may inquire about withdrawing their dissertation and/or thesis from this database. For additional inquiries, please contact the repository administrator via email ([scholarship@uwindsor.ca](mailto:scholarship@uwindsor.ca)) or by telephone at 519-253-3000ext. 3208.

**COMPARATIVE STUDY OF JOINT STIFFNESS  
CALCULATIONS USING THE FINITE ELEMENT  
ANALYSIS**

by

Negar Rasti

A Thesis  
Submitted to the Faculty of Graduate Studies and Research  
Through Mechanical Engineering  
In Partial Fulfillment of the Requirements for  
The Degree of Master of Applied Science at the  
University of Windsor

Windsor, Ontario, Canada

2007

©2007 Negar Rasti



Library and  
Archives Canada

Bibliothèque et  
Archives Canada

Published Heritage  
Branch

Direction du  
Patrimoine de l'édition

395 Wellington Street  
Ottawa ON K1A 0N4  
Canada

395, rue Wellington  
Ottawa ON K1A 0N4  
Canada

*Your file* *Votre référence*  
*ISBN: 978-0-494-35058-4*  
*Our file* *Notre référence*  
*ISBN: 978-0-494-35058-4*

**NOTICE:**

The author has granted a non-exclusive license allowing Library and Archives Canada to reproduce, publish, archive, preserve, conserve, communicate to the public by telecommunication or on the Internet, loan, distribute and sell theses worldwide, for commercial or non-commercial purposes, in microform, paper, electronic and/or any other formats.

The author retains copyright ownership and moral rights in this thesis. Neither the thesis nor substantial extracts from it may be printed or otherwise reproduced without the author's permission.

**AVIS:**

L'auteur a accordé une licence non exclusive permettant à la Bibliothèque et Archives Canada de reproduire, publier, archiver, sauvegarder, conserver, transmettre au public par télécommunication ou par l'Internet, prêter, distribuer et vendre des thèses partout dans le monde, à des fins commerciales ou autres, sur support microforme, papier, électronique et/ou autres formats.

L'auteur conserve la propriété du droit d'auteur et des droits moraux qui protègent cette thèse. Ni la thèse ni des extraits substantiels de celle-ci ne doivent être imprimés ou autrement reproduits sans son autorisation.

---

In compliance with the Canadian Privacy Act some supporting forms may have been removed from this thesis.

Conformément à la loi canadienne sur la protection de la vie privée, quelques formulaires secondaires ont été enlevés de cette thèse.

While these forms may be included in the document page count, their removal does not represent any loss of content from the thesis.

Bien que ces formulaires aient inclus dans la pagination, il n'y aura aucun contenu manquant.

  
**Canada**

## ABSTRACT

The focus of this work is on the calculation of the member stiffness of bolted joints. Three different types of joints were discussed according to the methods of loading, which are: Conventional Joints, Axisymmetric Loaded Joints and Eccentrically Loaded Joints

Separate simulations were performed for each of the three different types of joints. A new analytical method was introduced for studying the connections. This method takes into consideration the member stiffness reduction associated with the residual force, compression deformation caused by the external load itself and member dimension change due to the member rotation. Stiffness of the conventional joints can be calculated if the new analytical method's factors were neglected.

Different limitations of simulating the joint connections were studied in the simple form of conventional joints. For the joints under the compressive and transvers loading the best accuracy were achieved by modeling all parts of the joints including all parts of the bolt and the interactions between them. In axisymmetric joints these issues can replace the model without any effect on the accuracy of the system

The effect of washer in the joint connections is also studied which shows how washer can localize the effect of the compressive load in the connections without having a significant change on the stiffness of the joint.

Calculation of the load location factor is also determined in this study and the results were compared with the results reported in VDI 2230 (The German Structural Code). The calculated values from this study show the lower value compared to the VDI, due to the fact that in this study, the external load is applied on the members more realistically. In VDI the applied force is applied exactly at the bolt axis, which is not the case in real problems.

## DEDICATION

To my husband and my parents

## ACKNOWLEDGEMENTS

I would like to thank my supervisor, Dr Zamani for his comments on my thesis and his guidance during the formation of this thesis. In addition, I also like to thank Dr Altenhof and Dr Budkowska for their helpful comments and suggestions.

## TABLE OF CONTENTS

ABSTRACT	iv
DEDICATION	v
ACKNOWLEDGEMENTS	vi
LIST OF TABLES	vii
LIST OF FIGURES	ix
NOMENCLATURE	xii
<b>CHAPTER</b>	
<b>1. INTRODUCTION</b>	<b>1</b>
Motivation for This Work	1
Basic Methodology of Calculating the Joint Stiffness	4
Bolt Stiffness Calculation	4
Member Stiffness Calculation	5
Conventional Theory	5
Analytical Method of Calculating Axisymmetric Loaded Joints	8
Prying Action	11
Different Modes of T-Stub Failure	12
<b>2. LITERATURE REVIEW</b>	<b>14</b>
Conventional Joints	14
Axisymmetric Externally Loaded Joints	19
Eccentrically Loaded Joints	21
<b>3. COMPARATIVE STUDY OF DIFFERENT CONVENTIONAL BOLTED JOINTS AND THEIR LIMITATIONS</b>	<b>27</b>
Model Description	27
Finite Element Model	28
Finite Element Results	33
Energy Balance Study of the Model	35
Effect of Having a Washer in the Resultant Stiffness	37
Discussion of the Results	38

<b>4. INVESTIGATING ZHANG'S THEORY BY SIMULATING</b>	
<b>AXISYMMETRIC LOADED JOINTS</b>	41
Load Location (Plane) Factor Definition	41
Finite Element Model Description	43
Finite Element Results	44
Calculating the Loading Plane Factor Using Zhang's Model	46
Discussion of the Results	49
<b>5. NEW ANALYTICAL METHOD FOR STUDYING ECCENTRICALLY</b>	
<b>LOADED JOINTS</b>	51
Introduction	51
Studying the Behavior of T-Stubs	51
Model Description	54
Finite Element Modes	55
Correlation of the Model with Bursi's Results	56
Analytical Calculation of Member Stiffness According to the Zhang's	
Model for a Specific Example	59
Member Stiffness Calculation at Preload	59
Calculation of the Member Stiffness of Externally Loaded Joints	61
Calculating the Joint Stiffness for Different Applied Loading	71
Discussion of the Results	73
<b>6. CONCLUSIONS, AND RECOMMENDATIONS</b>	75
<b>REFERENCES</b>	80
<b>APPENDIX A: Calculation of the Joint Stiffness from Different Theories for</b>	
<b>One Specific Problem</b>	84
<b>APPENDIX B: Tips for Modeling Bolt in Finite Element Analysis</b>	87
<b>APPENDIX C: Displacement of the Member Depicted on Nine Different</b>	
<b>Paths</b>	95
<b>VITA ACTORIS</b>	97



## LIST OF TABLES

Table 3.1	Geometries and Preload Values [Maruyama et. al (1975)]	28
Table 3.2	Material Properties of the Connection [Maruyama et. al (1975)]	28
Table 3.3	Convergence Criteria for Each Mesh Density	32
Table 3.4	Comparison of the Joint Stiffness Calculated in Different Studies	34
Table 3.5	The Strain Energy and Stiffness for Each Part of the Connection	36
Table 4.1	Locations of the Applied External Load	43
Table 4.2	Joint Stiffness Values from 2D and 3D Analysis	45
Table 4.3	Different Deformations Measured from FEA	46
Table 4.4	Different Factors of Analytical Model	47
Table 4.5	Load Factor and Load Location Factor at Each Point	48
Table 5.1	Material Properties of Each Part Associated with Our Model	55
Table 5.2	Convergence Criteria for Each Mesh Density	56
Table 5.3	The Bolt and Member Stiffness from the Finite Element Analysis and Conventional Theory	61
Table 5.4	The Measured Deformation for Applied Force of 40 kN	69
Table 5.5	Calculated Factors of New Analytical Model	71
Table 5.6	The Average Displacements for Different Applied Loads	72
Table 5.7	Different Factors Calculated for Different Applied Loads	72
Table 5.8	The Coefficient of Preload and Applied Force	72
Table 5.9	Comparing the Bolt Load from FEA and the New Analytical model	73

## LIST OF FIGURES

Figure 1.1	Three Different Types of Joints (a) Conventional Joint (b) Axisymmetric Loaded Joint (c) Eccentrically Loaded Joints	2
Figure 1.2	Components of the Typical Joint	4
Figure 1.3	The Frustum Area of the Member [Shigley et. al (2004)]	6
Figure 1.4	Deformation Measurements in Zhang's Method [Zhang and Poirier (2004)]	9
Figure 1.5	Schematic Model for Representing Prying Force [Kulak et. Al (1987)]	11
Figure 1.6	Three Modes of T-Stubs Failure (a) Yielding happened at the flange (b) Yielding happened at both bolt and flange (c) Failure of the bolt [Piluso et.al 2001]	13
Figure 2.1.	The FE Model Used by Wileman et.al (1991)	17
Figure 2.2	The FE Model Used by Lenhoff et.al (1994)	18
Figure 2.3	Allen's FE Model [Allen(2003)]	19
Figure 2.4	Finite Element Model Used by Gerbert and Bastedt (1993)	21
Figure 2.5	Finite Element Model Used by Bursi and Jaspart (1997,1998)	23
Figure 2.6	Different States for Bolt and Flange (Swanson 1999)	24
Figure 2.7	3-D Finite Element Model Used by Swanson et al. (2002)	25
Figure 2.8	2-D Finite Element Model Used by Swanson et al. (2002)	26
Figure 3.1	Solid 185 Geometry	29
Figure 3.2	(a) Pretension Geometry, (b) Pretension Definition [ANSYS (2003)]	30
Figure 3.3	Different Density of Mesh Used for Convergence Study (a) Mesh size 0.0064 (b) Mesh size 0.0032 (c) Mesh size 0.0016	31
Figure 3.4	TARGET170 Geometry [ANSYS (2003)]	33
Figure 3.5	Von Misses Stress Distributions in the Frustum Zone around the Bolt Hole	34
Figure 3.6	Strain Energy Driven from the Force-Displacement Curve	35
Figure 3.7	Schematic Model of the Joint with Washer	37
Figure 3.8	Stress Distributions in Presence of Washer	38
Figure 4.1	Load Plane Factor	42

Figure 4.2	Different Locations of the Applied External Load	44
Figure 4.3	The Stress Distribution in the Frustum zone Around the Bolt Hole	45
Figure 5.1	Flange Deformation Effect on Resultant Force Location [Kulak et. al (1987)]	52
Figure 5.2	Model Geometries in Bursi's Analysis [Bursi and Jaspart (1997)]	54
Figure 5.3	Different Density of Mesh Used for Convergence Study (a) Mesh size 4 mm (b) Mesh size 2 mm (c) Mesh size 1 mm	57
Figure 5.4	External Load vs. Displacement from Finite Element Results and the Previous Study	58
Figure 5.5	External Load vs. Bolt Load from FE Results and the Previous Study	58
Figure 5.6	The Frustum Stress Distribution Form at the Preload	59
Figure 5.7	Uniform Stress $\sigma_z$ (Pa) Distributions along the Bolt Hole	60
Figure 5.8	Different Views of Von Mises Stress Plot of Externally Loaded T-Stub	62
Figure 5.9	Counter Plots of Different Stress Components	63
Figure 5.10	The Flange Deformation on the Contact Area of Flange and Base	64
Figure 5.11	The Same Behavior of the Stress Distribution Around the Bolt Plotted Are Von Mises Stress (MPa) vs. Distance (mm)	65
Figure 5.12	The Difference Between the Total and the Vertical Deformation Counter Plot	66
Figure 5.13	The Equivalent Points of Measuring the Displacements (a) The schematic method of measuring the deflections from Zhang's model [Zhang and Poirier (2004)] (b) and (c) The path defined in this thesis for reading the desired deflection values	68
Figure B.1	Bolt under Different Types of Loading	88
Figure B.2	Hexahedron Element (a) First Order, (b) Second Order	89
Figure B.3	Different Bolt Characteristics	90
Figure C.1	Displacement of the Member Depicted on Nine Different Paths	96

## NOMENCLATURE

$d$	=	Diameter of bolt
$d_w$	=	Diameter of bolt head or washer
$d_h$	=	Diameter of bolt hole
$t$	=	Thickness of each compression member
$\delta$	=	Member Displacement
$L$	=	Length of the members
$\sigma_z$	=	Stress component in z direction
$A$	=	Area of each axially loaded member
$A_{eq}$	=	equivalent cross section of the distributed stress
$A_b$	=	Cross section area of the bolt
$t_h$	=	Thickness of the bolt head
$\alpha$	=	Angle of the frustum
$D$	=	Diameter of the member
$r_0$	=	Outside diameter of the frustum
$r_i$	=	In side diameter of the frustum
$w$	=	Width of the T- stub per each bolt
$m$ and $n$	=	Distance between the bolt axis, to the web base and flange tip respectively
$E$	=	Young's Modulus
$\nu$	=	Poisson's Ratio
$C$	=	Load factor
$C_n$	=	Load factor for an arbitrary location of external load
$n$	=	Load location factor
$f_u$	=	Ultimate stress
$f_y$	=	Yield stress
$F_i$	=	Preload force
$F_b$	=	Bolt load
$F_{res}$	=	Residual fore

$F$	=	External force
$F_{sep}$	=	Minimum external load that causes joint separation
$T$	=	Externally tensile Load
$\beta_{u,lim}$	=	Collapse mechanism topology
$K'_m$	=	Dimensionless form of $\frac{K_m}{E_m d}$
$K_b$	=	Bolt stiffness
$K_t$	=	Stiffness of the threaded part of bolt
$K_d$	=	Stiffness of the unthreaded part of bolt
$K_m$	=	Member stiffness at preload
$K_c$	=	Member cylinder stiffness
$K_m(F)$	=	Varying member stiffness
$K_{m,\theta}$	=	Member rotation stiffness
$a$	=	Proportional factor
$C$	=	Load factor
$\delta_b$	=	Bolt deformation
$\delta_m$	=	Member deformation
$\delta_{m,F}$	=	Member deformation cause by external force
$\delta_{m,F_i}$	=	Member deformation at preload
$\delta_{m,res}$	=	Member deformation cause by residual force
$\delta_\theta$	=	Member deformation seen by the bolt cause by the member rotation
$\Delta_b$	=	Additional bolt deformation when external load in present
$\Delta_m$	=	Additional member deformation when external force is present
$\Delta_{m,res}$	=	Additional member deformation due to residual force
$A(F)$	=	Coefficient of the preload

- $B (F)$  = Coefficient of the external load
- A = Wileman and Choudhury's numerical constant defined for each material
- B = Wileman and Choudhury's numerical constant defined for each material

# CHAPTER ONE

## INTRODUCTION

### 1.1 Motivation for This Work

Bolted connections are used in different mechanical assemblies. Studying the stiffness of the connection is important to find the response of the assembled connection when subjected to an external loading. A great deal of research has been performed for studying the stiffness of preloaded joints. The analytical solution for the preloaded joints has been discussed as conventional theory by many researchers. The conventional theory provides basic insight into the bolt behaviour, however the actual behaviour of the joints are much more complicated than the conventional theory. The theory does not take into account if the external force was applied to the connection, in addition to the pretension. Only few studies have been done for solving the analytical solution of axisymmetric loaded joints which do not have the limitations of conventional theory. No studies have been done for investigating the analytical solution of the eccentrically loaded joints.

The objective of this study is to establish an analytical method for calculating the joint stiffness of any type of joints. In this study, three different types of bolted connections are investigated to calculate their member stiffness. Figure 1.1 shows different types of loading of each type of joint. The joints are categorized according to the method by which the loads are applied. These three types are mentioned as follows:

- a) Conventional joints, in which the load is applied at the bolt axis (Figure 1.1.a)
- b) Axisymmetric loaded joints, in which the axisymmetric load is applied at some distance from the bolt axis (Figure 1.1.b)
- c) Eccentrically loaded joints, in which the eccentrically load is applied at some distance from the bolt axis (Figure 1.1.c)

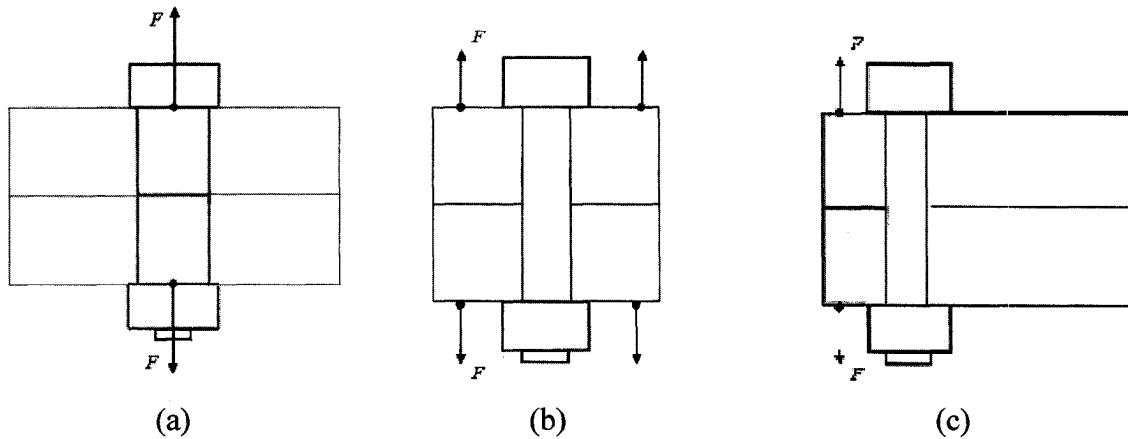


Figure 1.1 Three Different Types of Joints (a) Conventional Joint (b) Axisymmetric Loaded Joint (c) Eccentrically Loaded Joints

In conventional type of joints, the analytical method of calculating member stiffness is developed by assuming that the stress in the member is distributed in a frustum or cylindrical zone. Therefore, by having the area of the distributed stress, the member stiffness can be easily calculated.

Zhang and Poirier (2004), were the pioneers who introduced the analytical method for calculating the member stiffness of axisymmetric loaded joints. The theory will be referred as the Zhang's model in the rest of this study. Zhang's model could easily be used for studying conventional joints.

In order to establish a specific study for calculating the member stiffness for each type of joints, we need to investigate if Zhang's model could also be used for predicting the member stiffness of eccentrically loaded joints. To investigate this issue, a T-stub connection is considered for the eccentrically loaded joints. Zhang's theory is used to calculate the stiffness of T-stub model around its joint. The strengths and the weaknesses of using the Zhang's generalized model approach in all types of joints are also studied.

The chapters are organized in the following order:



1. Chapter one is the introduction containing the basic methodology for calculating the joint stiffness followed by scrutinizing the conventional theory and the Zhang's model. The analytical issues regarding the T-stub connections are also considered in the introduction.
2. Chapter two is the literature survey dealing with the calculation of the joint stiffness. The literature reviews are categorized in three different sections for each type of joint.
3. In chapter three different simulations have been done to study the joints with conventional theory limitations. The stiffness of the joints will be calculated and compared to the other previous studies of the same problem but with different types of modeling. The effect of washers in connections is also studied in this chapter. At the end the energy balance study has been conducted to investigate the energy equilibrium of the analysis.
4. In chapter four a finite element analysis is performed by considering the theory of the analytical model of the bolted joints introduced by Zhang and Poirier (2004). The load location factor is also introduced and calculated analytically and the results were compared with the predicted values.
5. Chapter five is the main contribution of the author. In this chapter, the accuracy of Zhang's model is determined for eccentrically loaded joints. A T-stub connection is considered to investigate if the new model can be used to explain the behavior the joint, this includes the bolt load and the deformations that cause the stiffness.
6. Chapter six includes conclusions and recommendations.

## 1.2 Basic Methodology of Calculating the Joint Stiffness

The stiffness of an axially loaded member  $K_m$  can be expressed by dividing the force  $F$  over the displacement of the member  $\delta$  according to equation 1.1:

$$K_m = \frac{F}{\delta} = \frac{AE}{L} \quad (1.1)$$

$A$ ,  $E$ , and  $L$  are area, Young's Modulus and length of the member respectively.

A typical joint is composed of two components, a bolt and the members shown in figure 1.2. Each part in the member acts like a spring and the stiffness of each part can be calculated according to the equation 1.1. Calculating the stiffness of sets of parallel or series springs will lead to the overall stiffness of the joint.

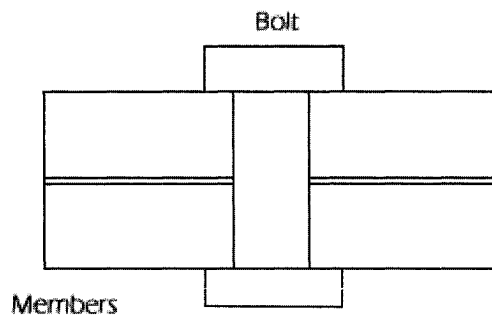


Figure 1.2 Components of the Typical Joint

## 1.3 Bolt Stiffness Calculation

Bolts generally consist of two distinct sections, the threaded and the unthreaded sections. The overall stiffness of the bolt is determined by modeling each segment as a spring. The overall stiffness is determined from the equation 1.2, where  $K_t$  and  $K_d$  are the stiffnesses of the threaded and unthreaded parts.

$$\frac{1}{K_b} = \frac{1}{K_t} + \frac{1}{K_d} \quad (1.2)$$

In many studies, only the unthreaded bolt is considered, especially when the results are compared with the numerical simulations with unthreaded bolts.

#### **1.4 Member Stiffness Calculation**

The stiffness of the member is determined by considering the effective spring stiffness of the member components. For joints with multiple members, this is accomplished by considering a number of springs in series. For a joint consisting of  $n$  members, the equation 1.4 presents:

$$\frac{1}{K_m} = \frac{1}{K_1} + \frac{1}{K_2} + \dots + \frac{1}{K_n} \quad (1.3)$$

The member stiffness calculation is much more complex. It is not possible to find the effective area in the calculation of the stiffness. There are some assumptions for approximating these effective areas. For instance, the effective area can be approximated as the frustum or the cylindrical area, which is discussed in the next section.

#### **1.5 Conventional Theory**

Conventional theory deals with symmetric joints. In symmetric joints, external load is applied at the bolt's head or at the interface of the bolt shank.

The complicated calculation of the member stiffness is simplified by some assumptions. One of the assumptions is that the stress distribution of the member is in the frustum area as shown in figure 1.3.

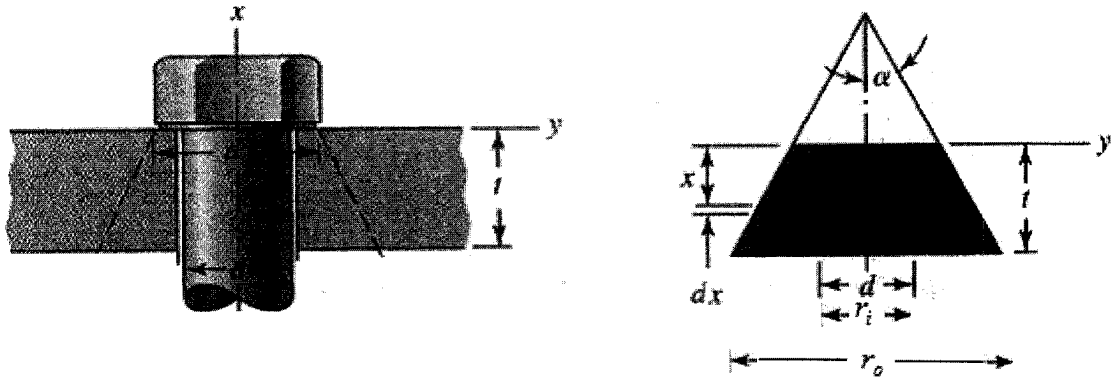


Figure 1.3 The Frustum Area of the Member [Shigley et. al (2004)]

The stiffness is then calculated according to the equation 1.1.

The change in the length of each element of the cone of thickness  $dx$  subjected to a compressive force of  $F$  is derived from the equation 1.4.

$$d\delta = \frac{Fdx}{EA} \quad (1.4)$$

The area of the element  $A$  is calculated according to the equation 1.5. Here  $r_o$  and  $r_i$  are the inside and outside radius of the frustum. The variable  $r_i$  is equal to the diameter of the bolt that is equal to the member hole.

$$A = \pi(r_o^2 - r_i^2) \quad (1.5)$$

According to figure 1.3, the equations 1.6 and 1.7 will be formed. The angle  $\alpha$  is the fixed angle between the surface of the cone and the centerline of the bolt.

$$A = \pi \left[ \left( x \tan \alpha + \frac{d_w}{2} \right)^2 - \left( \frac{d}{2} \right)^2 \right] \quad (1.6)$$

$$A = \pi \left[ x \tan \alpha + \frac{d_w + d}{2} \right] \left[ x \tan \alpha + \frac{d_w - d}{2} \right] \quad (1.7)$$

Substituting the area from equation 1.7 into equation 1.4 and integrating will form the total contraction as, equations 1.8,

$$\delta = \frac{F}{\pi E} \int_0^t \frac{dx}{\left[ x \tan \alpha + (d_w + d)/2 \right] \left[ x \tan \alpha + (d_w - d)/2 \right]} \quad (1.8)$$

After integrating equation 1.8, we can derive equation 1.9 according to

$$\delta = \frac{F}{\pi E d \tan \alpha} \ln \frac{(2t \tan \alpha + d_w - d)(d_w + d)}{(2t \tan \alpha + d_w + d)(d_w - d)} \quad (1.9)$$

Therefore, the member stiffness can be calculated in equation 1.10.

$$K_m = \frac{F}{\delta} = \frac{\pi E d \tan \alpha}{\ln \frac{(2t \tan \alpha + d_w - d)(d_w + d)}{(2t \tan \alpha + d_w + d)(d_w - d)}} \quad (1.10)$$

The diameter of the washer face is about 50% larger than the bolt diameter. By substituting  $d_w = 1.5d$  in the equation 1.10, the equation is further simplified in equation 1.11.

$$K_m = \frac{\pi E d \tan \alpha}{2 \ln \left[ 5 \frac{2t \tan \alpha + 0.5d}{2t \tan \alpha + 2.5d} \right]} \quad (1.11)$$

If the two members are of equal thickness and they have the same Young's Modulus, then they act as two identical springs in series according to equation 1.12, which will form the final equation for each of the member stiffness.

$$\frac{1}{K_m} = \frac{1}{K_1} + \frac{1}{K_2} \quad (1.12)$$

## 1.6 Analytical Method of Calculating Axisymmetric Loaded Joints (Zhang's Model)

In the conventional method, the load is either applied at the bolt axis, the bolt head, or the member interface. However, the external load is usually applied at some distance from the bolt axis. By applying the external load at some distance, the compression force will be transmitted to the member, which will cause additional deformations.

Zhang and Poirier (2004) observed that when the external load is applied to the structure, external forces contribute to the additional member deformations, which can be seen by the bolt. None of these deformations are determined by the stiffness  $K_m$ . These additional deformations are consisting of one of the followings;

- Member compression due to external load  $\delta_{m,F}$
- Member thickness dimension change seen by the bolt, due to the member rotation  $\delta_{m,\theta}$
- Member expansion due to residual force relief  $\delta_{m,res}$

These deformations should be post processed from the finite element analysis. The method of extrating the results from finite element analysis is shown in figure 1.4. The entity  $\delta_{m,F}$  is the deformation caused by the external force only, measured when the joint is separated or when there is no pretension presented. The external load is transmitted via shear force, which produces the varying compression force. This compression force will cause  $\delta_{m,F}$ .

The deformation caused by the residual force will be affected by the reduction of the contact area. In order to calculate the  $\delta_{m,res}$  we first need to measure the total member deformation according to figure 1.4. By definition, the total member deformation is the summation of all member deformations as given in equation 1.13.

$$\delta_m = \delta_{m,F} + \delta_{m,res} + \delta_{m,\theta} \quad (1.13)$$

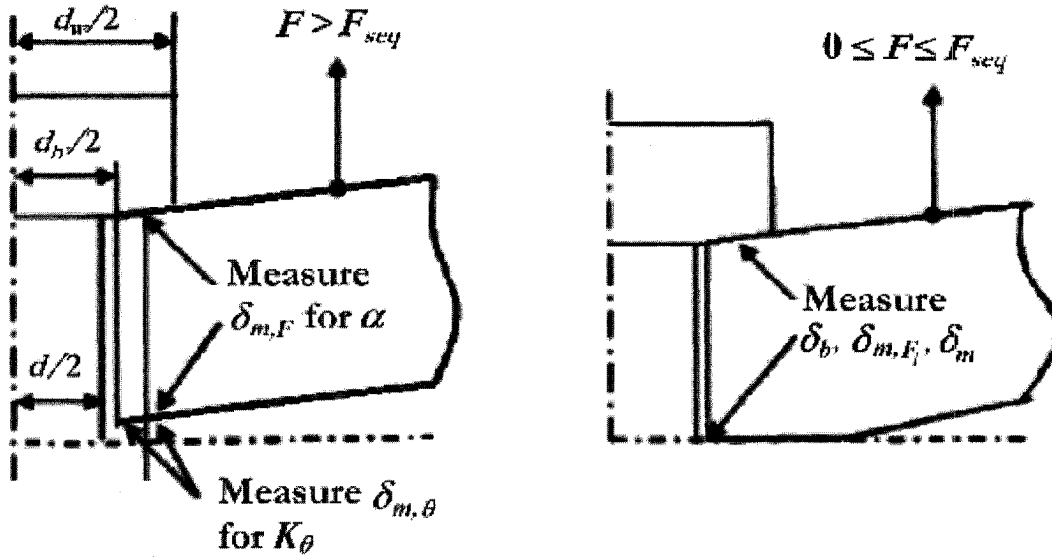


Figure 1.4 Deformation Measurements in Zhang's Method [Zhang and Poirier (2004)]

According to the above-mentioned deformations, three different factors will be introduced. Prior to their study, no one proposed methods for calculating these factors. These three new factors are: Proportional Factor, Member Rotation Stiffness and Varying Member Stiffness. These factors are described as follow;

- Proportional factor  $a$ : The factor  $a$  is a positive constant coefficient, which is defined in equation 1.14. This constant is considering the variation effects of the compression force transmitted from the external load  $F$ . (The factor denoted by  $\alpha$  in Zhang and Poirier study, however it will be shown as  $a$  in this study to avoid the confusion between the angle of frustum, which has been introduced in conventional theory)

$$a = -K_c \times \delta_{m,F} / F \quad (1.14)$$

In equation 1.14, the variable  $\delta_{m,F}$  is member deformation due to external load.  $F$  is the external load and  $K_c$  is the stiffness of cylinder, which is calculated in equation 1.15.

$$K_c = \pi(d_w^2 - d_h^2)E / 8t \quad (1.15)$$

- Member rotation stiffness  $K_\theta$ : The member rotation stiffness is calculated from equation (1.16)

$$K_\theta = F / \delta_{m,\theta} \quad (1.16)$$

Where  $\delta_{m,\theta}$  is the member rotation that is introduced in Zhang's model. The entity  $\delta_{m,\theta}$  is the deformation caused by rotation. It will be measured when the joint is separated. This parameter is actually representing the member dimension change seen by the bolt. To measure  $\delta_{m,\theta}$ , we should get the relative displacement between two points shown in figure 1.4.

- Varying member stiffness  $K_m(F)$ : The factor is calculating from equation 1.17

$$K_m(F) = -F_{res} / \delta_{m,res} \quad (1.17)$$

$F_{res}$  is residual force (compression force at member interface) and  $K_c$  is the cylinder stiffness. The varying member stiffness will be calculated from equation 1.18.

$$K_m(F) = F_{res} / (|\delta_m| + \delta_{m,F} + \delta_{m,\theta}) \quad (1.18)$$

By obtaining different displacements from finite element analysis results, the rotation stiffness, proportional factor, and the varying member stiffness can be calculated. Now



by substituting all these factors,  $A(F)$  and  $B(F)$  will be calculated from equations 1.19 and 1.20.

$$A(F) = (1 + K_m / K_b) / [K_m / K_m(F) + K_m / K_b] \quad (1.19)$$

$$B(F) = [1 - aK_m(F) / K_c + K_m(F) / K_\theta] / [1 + K_m(F) / K_b] \quad (1.20)$$

$A(F)$  and  $B(F)$  are the coefficients of preload and external load, which are functions of varying stiffness, member rotation stiffness, and the proportional factor. The bolt load  $F_b$  is also calculated according to the equation. 1.21.

$$F_b = A(F)F_i + B(F)F \quad (1.21)$$

### 1.7 Prying Action

One of the significant characteristics of T-stubs is prying action. Prying forces  $Q$  are developed at the outer edges of the flange due to the bending effects in the T-stub flange. The prying force is the result of geometrical and material characteristics of the connected components. It is the major source for causing nonlinearity in T-stub connections.

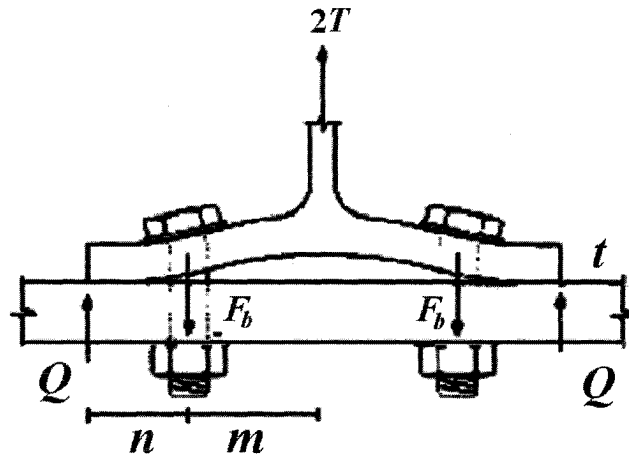


Figure 1.5 Schematic Model for Representing Prying Force [Kulak et. Al (1987)]

Analytical and experimental studies of prying action have been considered in several models and analysis. Douty and McGuire (1965) suggested a formula (Equation 1.22) based on an elastic analysis. Their equation relates the prying force to the ultimate load of the connection.

$$Q = \left\{ \frac{\frac{1}{2} - (wt^4 / 30nm^2 A_b)}{n/m[(n/3m) + 1] + (wt^4 / 6nm^2 A_b)} \right\} T \quad (1.22)$$

The entity  $w$  is the width of the T-stub per each bolt, and  $A_b$  is the cross section area of the bolt.  $n$  and  $m$  are the distances between the bolt axis to the flange tip and web base.  $T$  is the tensile load applied to the T-stub.

### 1.8 Different Modes of T-stubs Failure

By applying the tensile load to the T-stubs, the failure can be developed either at the flange to web intersection, at the bolt axis, or at both regions. According to the location of the appearing hinges, the T-stub connections are categorized into three modes of failure, which are shown in figure 1.6. These modes can be defined as:

- Mode 1: Yielding of the flange
- Mode 2: Yielding of the bolt and the flange
- Mode 3: This mode deals with the bolt failure

The collapse mechanism typology is governed by a parameter expressing the ratio between the flexural strength of the flange and the axial strength of the bolt as introduced by Piluso et. al (2001). The limit value of the mechanism typology parameter ( $\beta_{u,lim}$ ) is defined in equation 1.23, where  $\lambda = n/m$ . The variables  $m$  and  $n$  are shown in figure 1.5.

$$\beta_{u,\text{lim}} = \frac{2\lambda}{1+2\lambda} \left[ 1 - (1+\lambda) \frac{d_w}{8n} \right] \quad (1.23)$$

- T-stubs could be designed to have a specific mode according the parameter mentioned in equation 1.26 (collapse mechanism typology). The mode selected is based on the value of  $\beta_{u,\text{lim}}$ , according to the criteria in equations 1.24.

- Mode 1 is selected if  $\beta_{u,\text{lim}} < 2/3$
  - Mode 2 is selected if  $2/3 < \beta_{u,\text{lim}} \leq 2$
  - Mode 3 is selected if  $\beta_{u,\text{lim}} > 2$
- (1.24)

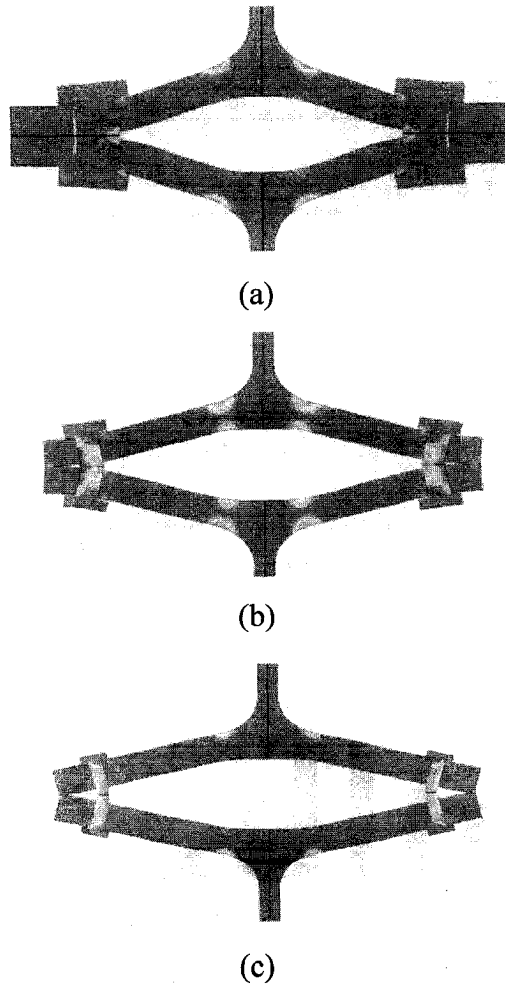


Figure 1.6 Three Modes of T-Stubs Failure (a) Yielding happened at the flange (b) Yielding happened at both bolt and flange (c) Failure of the bolt [Piluso et.al 2001]

## CHAPTER TWO

### LITERATURE REVIEW

This literature review includes related studies for understanding the stiffness of bolted joints. This review is categorized into three different parts corresponding to the three different groups of the joints considered in our study. In each part, both analytical and finite element analysis were discussed.

#### 2.1. Conventional Joints

In this section, the studies, with the classical joints assumptions, are considered.

Meyer and Strelow (1972) suggested that the stresses in the members due to the compression are distributed in a hollow cylinder zone. They developed equation 2.1 for calculating the equivalent cylinder's cross-sectional area.

$$A_{eq} = \frac{\pi}{4} \left[ \left( d_w + \frac{t}{10} \right)^2 - d^2 \right] \quad (D > 3d_w, t < 8d) \quad (2.1)$$

$A_{eq}$  is the equivalent cross section of the distributed stress,  $d$ ,  $d_w$ , and  $D$  are the bolt, washer and the member diameters respectively and  $t$  is the thickness of the members.

Edwards and McKee (1972), and Bickford (1995) cited the association of German engineers' suggestions to determine the area under compression. They also considered the cylindrical theory and suggested that the equivalent cylindrical area depends on the size of the joint.

Rötscher (1927) was the first to propose that the stresses were contained within two conical frusta, symmetric around the mid plane of the joint each having a vertex angle of  $2\alpha$ . He suggested that the cone angle depended on the material. He then chose  $\alpha = 45^\circ$  and computed stiffness by replacing the frustum with cylinder with the same average diameter according to equation 2.2.

$$K_m = \frac{\pi E}{4L} \left[ \left( d_w + \frac{L}{2} \right)^2 - d^2 \right] \quad (2.2)$$

$K_m$  is the stiffness of member,  $L$  is the length of each member,  $d$  and  $d_w$  are the bolt and washer diameters.

Ito et.al (1979) used ultrasonic techniques to determine the pressure distribution. He suggested that the proper value for  $\alpha$  depends on the material. They also provided a table of suggested values for  $\alpha$ . According to their results, the pressure is considerable, in about 1.5 bolt radius zone. Therefore, they suggested the use of the pressure cone method developed by Rötcher (1927) for stiffness calculation with variable cone angles.

Little (1967) and Osgood (1972) suggested the use of an angle smaller than  $45^\circ$  (i.e.,  $30^\circ$ ). Little reported that using an angle of  $45^\circ$ , overestimates the clamping stiffness. He suggested that for the common material (hardened steel, cast iron, or aluminum), the proper angle is smaller. Osgood reported the range of  $25^\circ \leq \alpha \leq 30^\circ$  for most of the materials.

Shigley and Mitchell (1983) assumed that the compressive load on the member is applied by a washer with the diameter of  $d_w = 1.5d$ . They simplified the model according to equation 2.3.

$$K_m = \frac{\pi E d}{2 \ln \left( 5 \frac{L + 0.5d}{L + 2.5d} \right)} \quad (2.3)$$

Shigley and Mischke (1995) stated that the angle  $\alpha$  is a variable. They recommended an angle of  $30^\circ$ . The resulting stiffness is mentioned in equation 2.4.

$$K_m = \frac{0.577\pi Ed}{2 \ln \left( 5 \frac{0.577L + 0.5d}{0.577L + 2.5d} \right)} \quad (2.4)$$

Motosh (1976) suggested the most realistic technique. He assumed that the stress in any plane perpendicular to the axis is maximum at the hole and decreases continuously to zero at the boundary of the conical zone. The compressive stress in the member is described by a fourth order polynomial depending upon  $d$ ,  $t$ , and  $\alpha$ . The stiffness is then computed using a series of numerical integrations. This method is not commonly used and is too complicated for the routine joint design.

Wileman et.al (1991) conducted a finite element study for different models of bolted joints with different geometry and material values. They suggested a dimensionless exponential expression to determine an equation for calculating the member stiffness. Their formula has been correlated to the finite element results performed by them.

They considered two symmetric boundary conditions; symmetric axis and symmetric plane. This way, they could use a two-dimensional finite element method to perform their calculations. They used ANSYS for their simulations. Their finite element model is shown in figure (2.1). Their analysis was limited to members of the same material for a condition that slippage does not occur at the interface between these members. The elastic modulus of the washer was defined to be approximately three order of magnitude of the member's Young's Modulus, so that the washer becomes almost rigid and the displacement of the members is uniform across the interface of the washer. They obtained a relationship between dimensionless stiffness  $\frac{K_m}{Ed}$  and aspect ratio  $d/L$ , which is shown in equation 2.5.

$$\frac{K_m}{Ed} = A \exp(Bd/L) \quad (2.5)$$

In the above equation  $A$  and  $B$  are dimensionless coefficients dependent on the member material.  $D$  is the diameter of the bolt,  $K_m$  and  $L$  are the stiffness and the length of the members and  $E$  is the Young's modulus of the bolt and members.

Wileman provided tables with values for the coefficients  $A$  and  $B$  based on curve fitting schemes. They found that their results were close to that of Shigley and Mischke (1995) model using  $\alpha = 30^\circ$ .

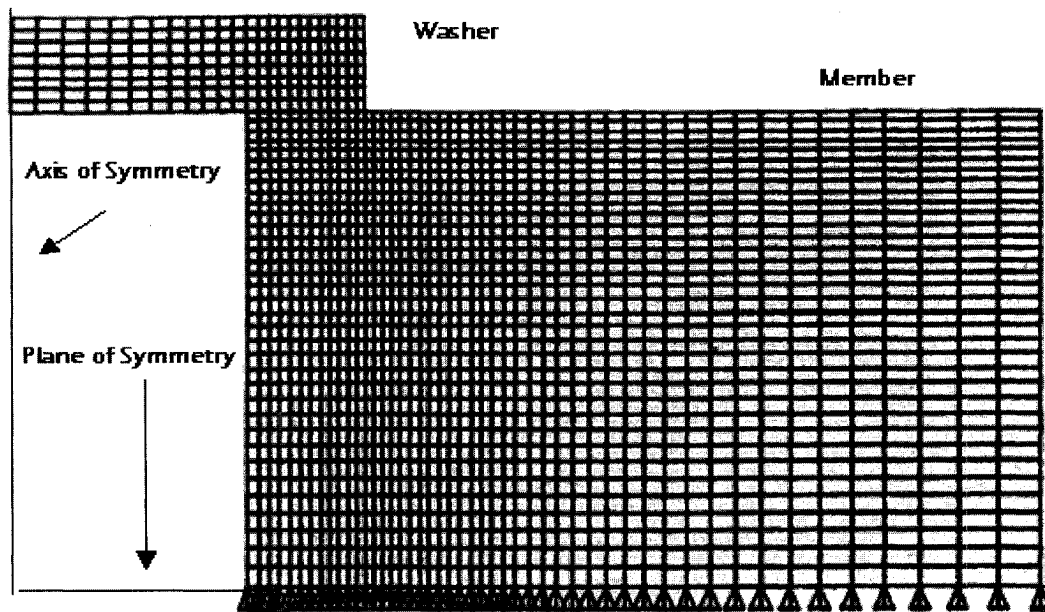


Figure 2.1. The FE Model Used by Wileman et.al (1991)

Lenhoff et.al (1994) also used a two-dimensional finite element model to calculate the member stiffness and the stress distribution in the bolts and the member. Because of the symmetry, only half of the joint was modeled. Axisymmetric and quadratic elements were used. Figure 2.2 shows the finite element model developed by them. They observed a slight separation between two members of the joint. The average displacement of the nodal points along the contacting portion was used to calculate stiffness of members. They used different materials and various combinations of thicknesses for members of the joint. Their results were very close to the one calculated by the basic theory, where a fixed cone angle of smaller than  $30^\circ$  could be used.

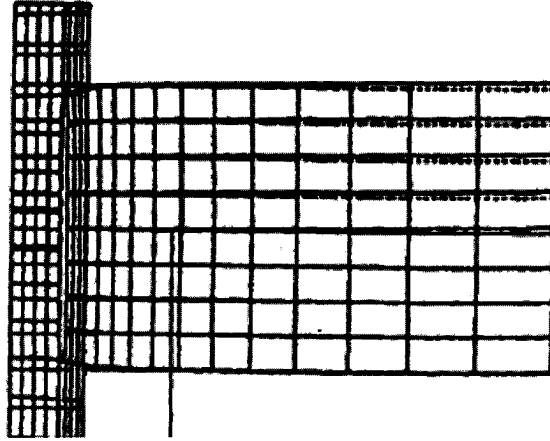


Figure 2.2 The FE Model Used by Lenhoff et.al (1994)

Their results were presented as a family of curves fitted into second order polynomial equations. Unique equations are presented for each member material combination (steel, aluminum and cast iron). Their equations, which are shown as equation 2.6, are based on the member length and bolt diameter. The first three equations are for various member materials. The fourth Equation fits into the modified 30° cone angle.

$$\left. \begin{aligned}
 k'_{m,steel} &= 0.05385291x^2 - 0.3933566x + 1.366381 \\
 k'_{m,al} &= 0.06089153x^2 - 0.04455611x + 1.516583 \\
 k'_{m,si} &= 0.05913646x^2 - 0.4895763x + 1.853846 \\
 k'_{m,shigley} &= 0.06061733x^2 - 0.4895763x + 1.853846
 \end{aligned} \right\} (2.6)$$

Where the  $K'_m$  is the dimensionless form of  $\frac{K_m}{E_m d}$  and  $x = L/d$ . The variables  $d$  and  $L$  are the diameter of the bolt and the length of the members respectively.



Allen (2003) determined the joint stiffness of preloaded bolted connections using strain energy calculations. Three-dimensional finite element analyses were used to model axisymmetric bolted joints. Bolt head geometry was modeled to account for the coupled bending stiffness at the bearing interface.

The bolted joints in his study were modeled by two types of 3D solid elements. A six-sided solid element representing the majority of the geometry and a five sided solid elements used in area of transition. Pretension was applied using the thermal strain technique. Figure 2.3 shows the Allen's finite element model. To simplify the analysis, only a section spanning  $5^\circ$  of the model was studied due to the symmetry. He was the first one who considered how the bolt and member stiffness could be calculated using the strain energy method.

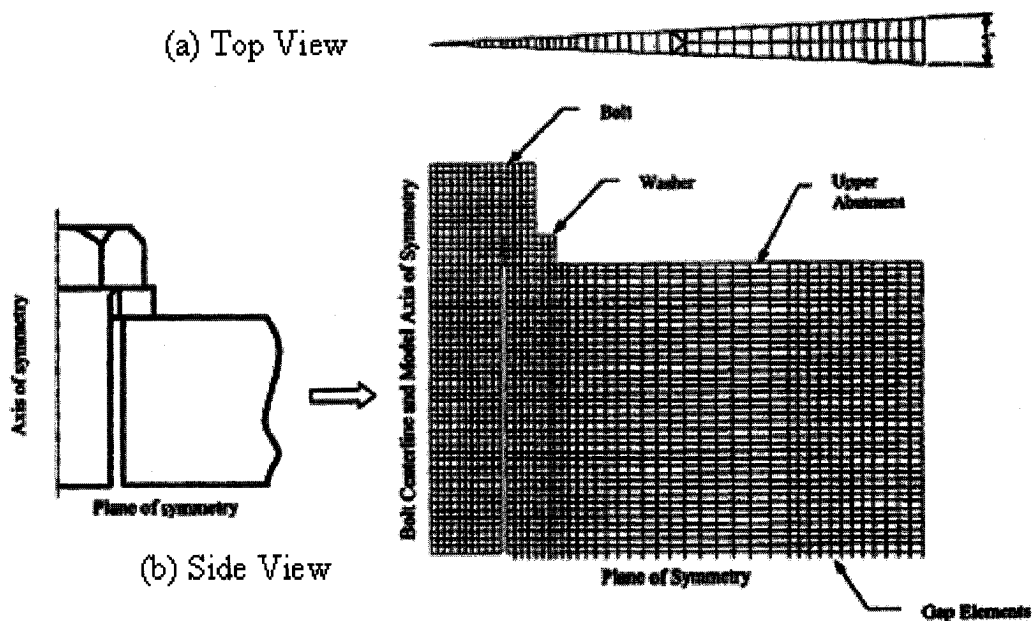


Figure 2.3 Allen's FE Model [Allen (2003)]

## 2.2. Axisymmetric Externally Loaded Joints

So far, the problems were pertaining to the conventional theory of bolted joint. In this section, the literature dealing with the axisymmetric loaded joint is discussed.

Zhang and Poirier (2004) have developed a new analytical model for studying the axisymmetric loaded joint. They believed that the new model of bolted joints would help them understand the joint behavior and serve as a base technique for the future research, analysis, and design.

According to their study, by applying the external load, additional member deformations might appear. These additional deformations are the member compression due to external load, member expansion and member thickness dimension change, seen by the bolt, due to member rotation.

According to these deformations, they have calculated three different factors. These three new factors are: member rotation stiffness, proportional factor, and varying member stiffness.

They have performed a finite element analysis to confirm their model. The agreement between the new analytical model and finite element result is excellent.

Gerbert and Bastedt (1993) evaluated the effects of the external load application located on a preloaded axisymmetric joint, using a finite element method. The model had a plane of symmetry perpendicular to the bolt axis. The preload was applied to the bolt by an enforced displacement at the plane of symmetry boundary, which is shown in figure 2.4. External loads were applied to various locations on the members. Due to the method of preload, they could measure the change in the bolt load (Basically the bolt load measured at each surface normal to the bolt axis) by the externally applied load. They also performed physical experiments to measure the effects of load application location.

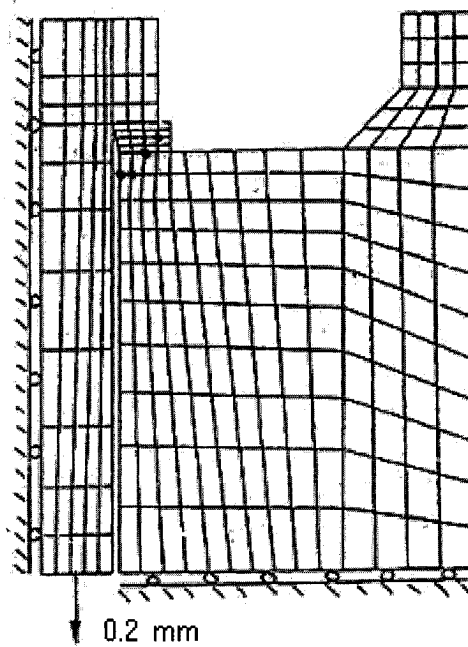


Figure 2.4 Finite Element Model Used By Gerbert and Bastedt (1993)

Gross and Mitchell (1990) also created an axisymmetric loaded bolted joint. They concluded that bolted joint stiffness is a function of externally applied load and is therefore nonlinear.

They applied a uniform thermal strain to the bolt in order to produce the desired preload. The thermal strain approach allows for a tension force to be developed in the bolt without using any externally applied forces or displacement.

### 2.3 Eccentrically Loaded Joints

Douty and McGuire (1965) studied the behavior of different T-stub models. A broad range of flange thickness's and bolt sizes were used to provide a robust data set to develop the calculation method of prying forces. An important conclusion of the work was the claim that T-stub connections can be designed to develop a full plastic moment in connected beams and that using thicker T-stub flanges reduces the effects of prying.

Their suggested formula for calculating the prying force is already discussed in chapter one.

Agerskov (1976) developed a model for the prediction of prying force, which is similar in to that of Douty and McGuire (1965). He used both equilibrium and compatibility equations to predict the prying forces. He provided a more sophisticated development of the bolt elongation. The possibility of using washers is also included in his study.

Choi and Chung (1996) employed a finite element methodology in the investigation of the behavioural characteristics of the end plate connections. In order to simulate the actual behaviour, a three dimensional model was established. The effect of the bolt pretension, the shape of the bolt shank, and the head and the nut are taken into consideration in the modeling. The gap elements were employed to simulate the interaction between the end plate and column flange. The prototype of an end plate connection was analyzed with the refined three dimensional finite element models and was verified by comparison with results from one particular test.

Bursi and Jaspart (1997, 1998) tested ten different T-stub components. They have presented different finite element studies depending on the constitutive relationships, step size, number of integration points, kinematics descriptions, element types, and discretizations, to show that the finite element programs can be used to accurately predict the behavior of the end plate connection.

Busri and Jaspart used the LAGAMINE software package, where the models are constructed using both hexahedron (commonly referred to as a “brick”) and contact elements. The contact elements utilize a penalty technique. The contact is simulated only for displacements within the given penalty value. The friction caused by the sliding and sticking between bodies was modeled with an isotropic Coulomb friction law. A nonlinear finite element analysis was used, which considers large displacements, large rotations, and large deformations. Loads were applied using displacement as the controlling parameter. When considering the bolts, the additional flexibility provided by

the nut and threaded region of the bolt, were taken into account using an effective length of the bolt. Due to the symmetry of the T-stub connection, only a quarter of the connection was modeled as shown in figure 2.5. Preloading forces in the bolts are taken into account using applied initial stresses. The material properties were modeled using linear constitutive laws for the material from experimentally tested connections. For several of these experimentally tested connections, finite element analysis was performed. The finite element results matched well with the experimental results.

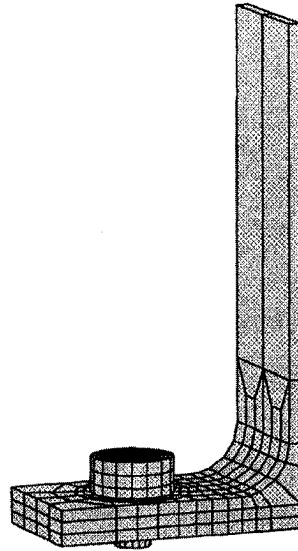


Figure 2.5 Finite Element Model Used By Bursi and Jaspart ( 1997,1998)

Sherbourne, and Bahaari (1996) conducted a three-dimensional finite element analysis to study the stiffness and strength of the T-stubs. A three-dimensional finite element model of the four-bolt unstiffened extended end plate was developed using ANSYS (2003) codes. The bolt shank was modeled using *truss* elements and pretension was modeled as initial strain. The bolt head and the nut were also modeled. Contact elements were used to describe the end-plate interaction problem. Material nonlinearities were included in the analysis.

Swanson and Leon (2001) introduced a comprehensive study of T-stub connection. The model was based on spring theory, which incorporates the followings:

- Deformations from tension bolt elongation
- Bending of the T-stub flange
- Elongation of the T-stem
- Slip of the T-stub relative to the beam flange
- Bearing deformation of the T-stem, and
- Bearing deformation of the beam flange.

They studied bolt, stem, and flange stiffness separately and produced equations for different elastic and plastic mode. Formulation of the flange stiffness calculation was established according to different modes of flange deformation. By neglecting the yielding modes of the flange, bolt stiffness for the elastic-plastic condition was calculated for four different conditions shown in figure 2.6.

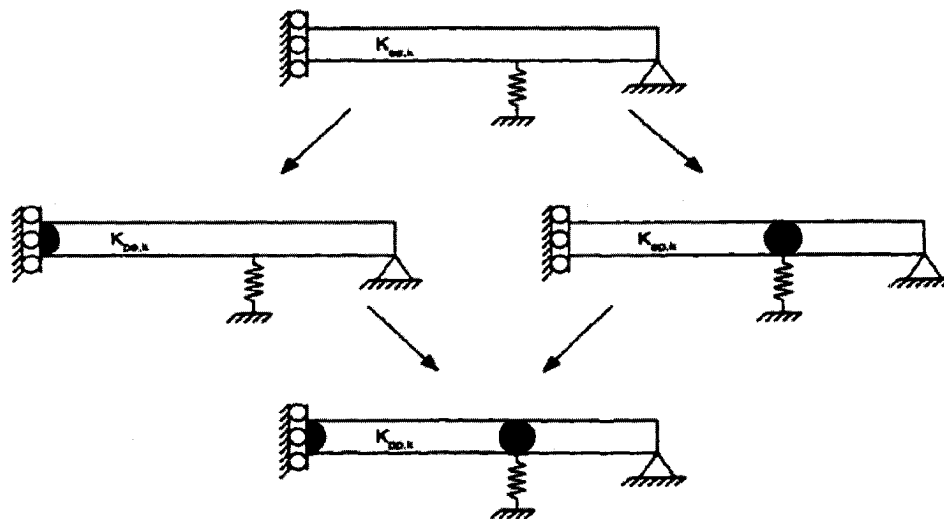


Figure 2.6 Different States for Bolt and Flange (Swanson 1999)

For each mode of the flange deformation, a specific equation was used. Swanson also introduced a different equation for the cases where the yielding might occur in the joint.

Swanson et.al (2002) conducted a finite element investigation of the T-stub flanges, which compared the results with the previous work done by Swanson and Leon. They have studied the following three models:

- The first model, which is shown in figure 2.7, was a 3D solid model incorporating contact with friction and full non-linear material properties. Although the 3D model proved to be computationally intensive, it provided valuable insight to the overall T-stub behavior including: pressure distributions on contact surfaces, two-dimensional plate bending behavior in the T-stub flange, and localized bending effects in the tension bolts.
- The second model, which is shown in figure 2.8 used 2D plane strain elements to model a unit width for the T-stub flange. This model also incorporated contact and full non-linear material properties and was used for studying the flange deformation characteristics.
- The third model used 2D plane stress elements to model the stem of a T-stub. Several behavioral characteristics were studied with this model including overall bolt bearing stiffness, stem stiffness, and stress distributions,

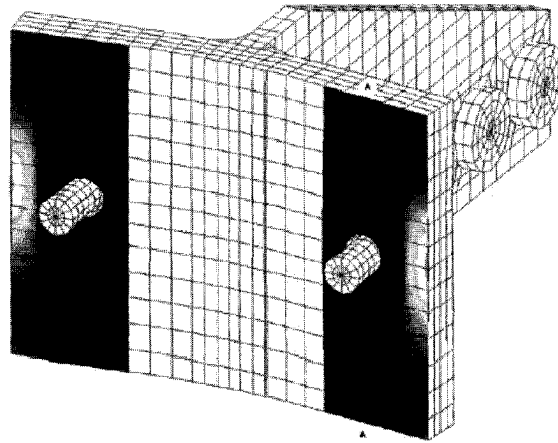


Figure 2.7 3-D Finite Element Model Used By Swanson et al. (2002)

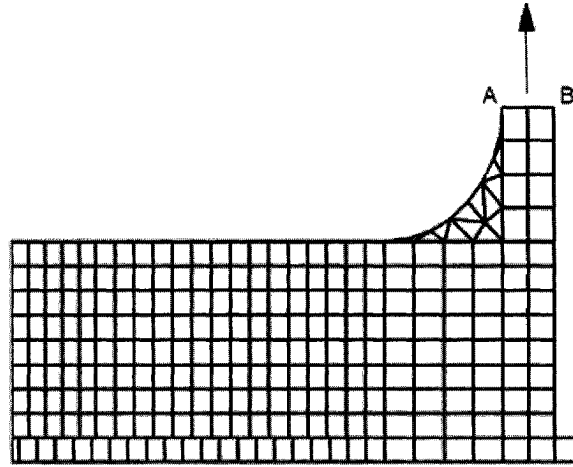


Figure 2.8 2-D Finite Element Model Used By Swanson et al. (2002)

Piluso et. al (2001) conducted both theoretical and experimental analysis for predicting the plastic deformation capacity of T-stubs. The corresponding formulations for predicting the ultimate value of the plastic displacement were given. Their model could also be used for an approximate evaluation of the whole force-displacement curve and predicting the stiffness. The collapse mechanism typology of T-stubs is analyzed by a parameter expressing the ratio between the flexural strength of the flange and the axial strength of the bolt, which was explained in chapter one.



# CHAPTER THREE

## COMPARATIVE STUDY OF DIFFERENT CONVENTIONAL BOLTED JOINTS AND THEIR LIMITATIONS

### 3.1 Model Description

In this chapter, a three-dimensional model is simulated to present a simple conventional model. The same model, which was studied by Wileman et.al (1991) and Lenhoff et.al (1994) will be studied. The differences between the results from this study and the results from previous models are discussed at the end of this chapter. The results are also compared with the experimental results and the conventional theory.

Wileman et. al (1991) studied a model, which contained both axis of symmetry and a plane of symmetry to reduce computational expenses, which is shown in figure 2.1. Since the stiffness of members is the only quantity to be considered, the shank of the bolt, bolt head, and nut have been removed from the model. Instead, the washer with elastic modulus of about three order of magnitude larger than that of the members is included.

They applied a surface pressure of  $17.24 \text{ MPa}$  to the stiff washer. The washer is essentially rigid and the deflection of the members is uniform. Wileman determined the effect of the joint geometry on the stiffness to establish a non-dimensional stiffness. To achieve this goal, he used different geometries.

For a numerical example, we calculated the stiffness for one of their models with the geometric properties identical to that of the experimental study of Maruyama et.al (1974).

The resulting stiffness can be compared to the experimental results. The geometric properties of the bolt and members are summarized in table 3.1. Unlike the Wileman's model, the bolt shank, head and the nut are also modeled. Both the bolt and the members are made of steel. The linear characteristic of steel material is given in table 3.2.

Table 3.1 Geometries and Preload Values [Maruyama et. al (1975)]

<b>Input Variables</b>	<b>Descriptions</b>	<b>Values</b>
$d$	Diameter of the bolt (mm)	24
$d_h$	Diameter of bolt hole (mm)	25
$d_w$	Diameter of the bolt head (mm)	$1.5d$
$D$	Member diameter (mm)	$D > 3d = 100$
$t$	Member thickness (mm)	25
$t_h$	Bolt head thickness (mm)	10
$F_i$	Preload force (kN)	10.572

Table 3.2 Material Properties of the Connection [Maruyama et. al (1975)]

<b>Material property</b>	<b>Young's Modulus</b>	<b>Poisson's ratio</b>
Steel	206.8 MPa	0.291

Some tips are given in Appendix B for modeling bolted joints to show how we can model a bolted connection in a finite element software package. Different methods for calculating the stiffness from FE results are also explained.

### 3.2 Finite Element Model

A three-dimensional model was simulated according to the above model descriptions. The whole structure including the bolt head, bolt shank and nut is modeled. The ANSYS code is used for our simulation.

The first step in modeling a bolted joint for determining the stiffness is to define a proper bolted joint region, which should be large enough to contain the stress distribution, and small enough not to include any significant portion of the structure. For this reason, member's diameter is selected to be at least three times of the bolt diameter.

A three-dimensional solid bolted joint including bolt head, nut, shank and both members is constructed. To simplify the problem, only half of the model (because of the symmetry) is simulated, which has no effect on the joint behavior. Contact could be

modeled by modeling both upper and lower plates. Modeling the bolt head and nut eliminates the use of the stiff washer. Linear isotropic material with the values that are given in table 3.2 is used for the study.

Slippage does not occur at the interface between the members. This no-slip requirement is always satisfied in joints that have equal thickness, which causes symmetric deflections. The assumption is only valid where the members have the same thicknesses and if the friction at the interface is sufficient to prevent slippage

The tetrahedral option of the SOLID185 element shown in figure 1.3, is used for modeling both bolt and members. SOLID185 is used for the 3-D modeling of solid structures. It is defined by eight nodes having three degrees of freedom at each node: translations in the nodal x, y, and z directions. The element has plasticity, hyperelasticity, stress stiffening, creep, large deflection, and large strain capabilities.

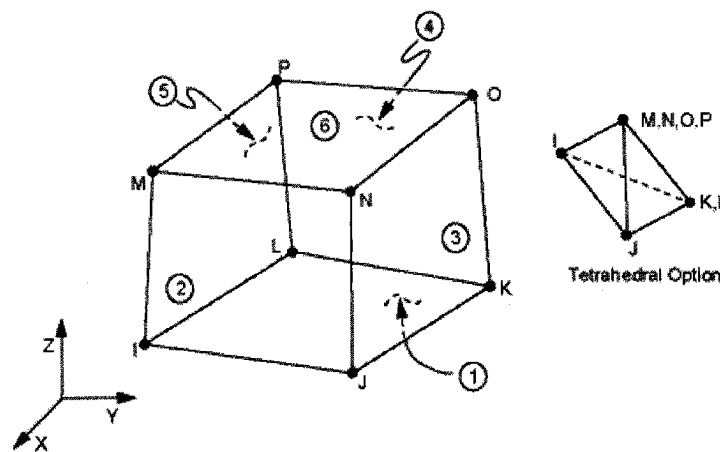


Figure 3.1 Solid 185 Geometry [ANSYS (2003)]

The pretension is defined through the pretension elements (PRETS179). The PRETS179 elements have one translation degree of freedom, which represents the defined pretension direction. ANSYS transforms the geometry of the problem so that, the pretension force is applied in the specified pretension load direction, regardless of how the model is defined

The pretension section is created through the elements in volume of the bolt. Pretension is applied by constant load, which is representing the compressive load applied by the washer in Wileman's study, which was 17.24 MPa. From the expression  $P = F / A$ , we can calculate the required pretension force by having the pressure and the area of the washer. Since only half of the geometry is modeled, therefore only half of the pretension force, which is equal to 5286 N, is applied.

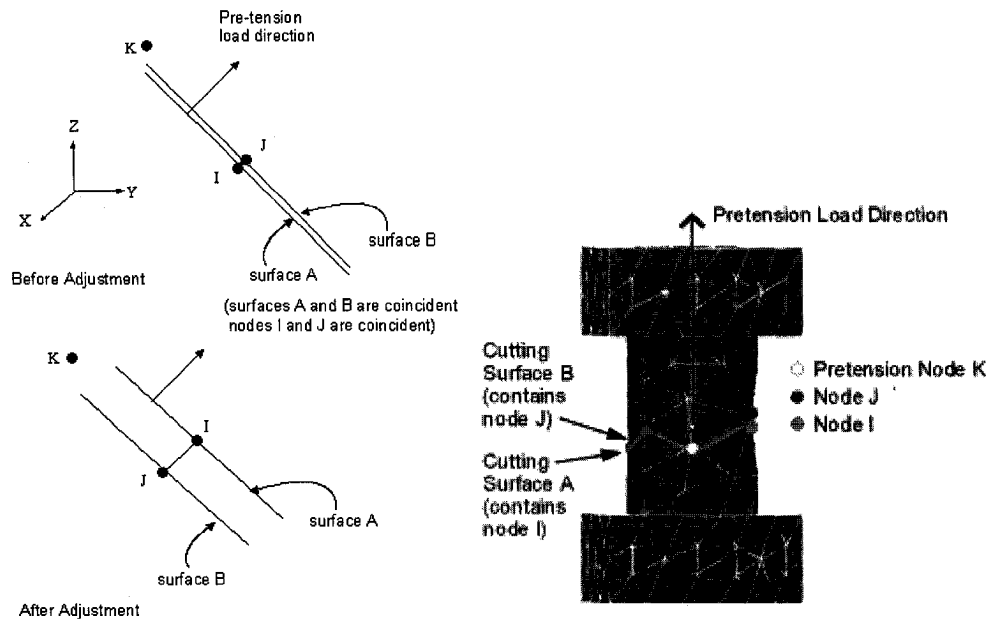


Figure 3.2 (a) Pretension Geometry, (b) Pretension Definition [ANSYS (2003)]

ANSYS defines the pretension through pretension elements by applying the initial load or applied displacements through PRETS179 elements shown in figure 3.2. Bolt can be made up of any 2-D or 3-D structural, low- or high-order solid, beam, shell, pipe, or link elements.

To define pretension in ANSYS we should first define the pretension section according to figure 3.2 and generate the pretension elements. It automatically cuts the meshed fastener into two parts and inserts the pretension elements. The pretension section must be defined inside the bolt part.

The convergence study has been done using different size of mesh. The analysis is converged at the mesh unit size of 0.0016 mm. Model includes approximately 69,000

nodes and 187,000 elements. Different mesh densities used for the study have been shown in figure 3.3. Table 3.3 represents and the maximum Von Mises stress selected as the convergence criteria for each of the mesh density.

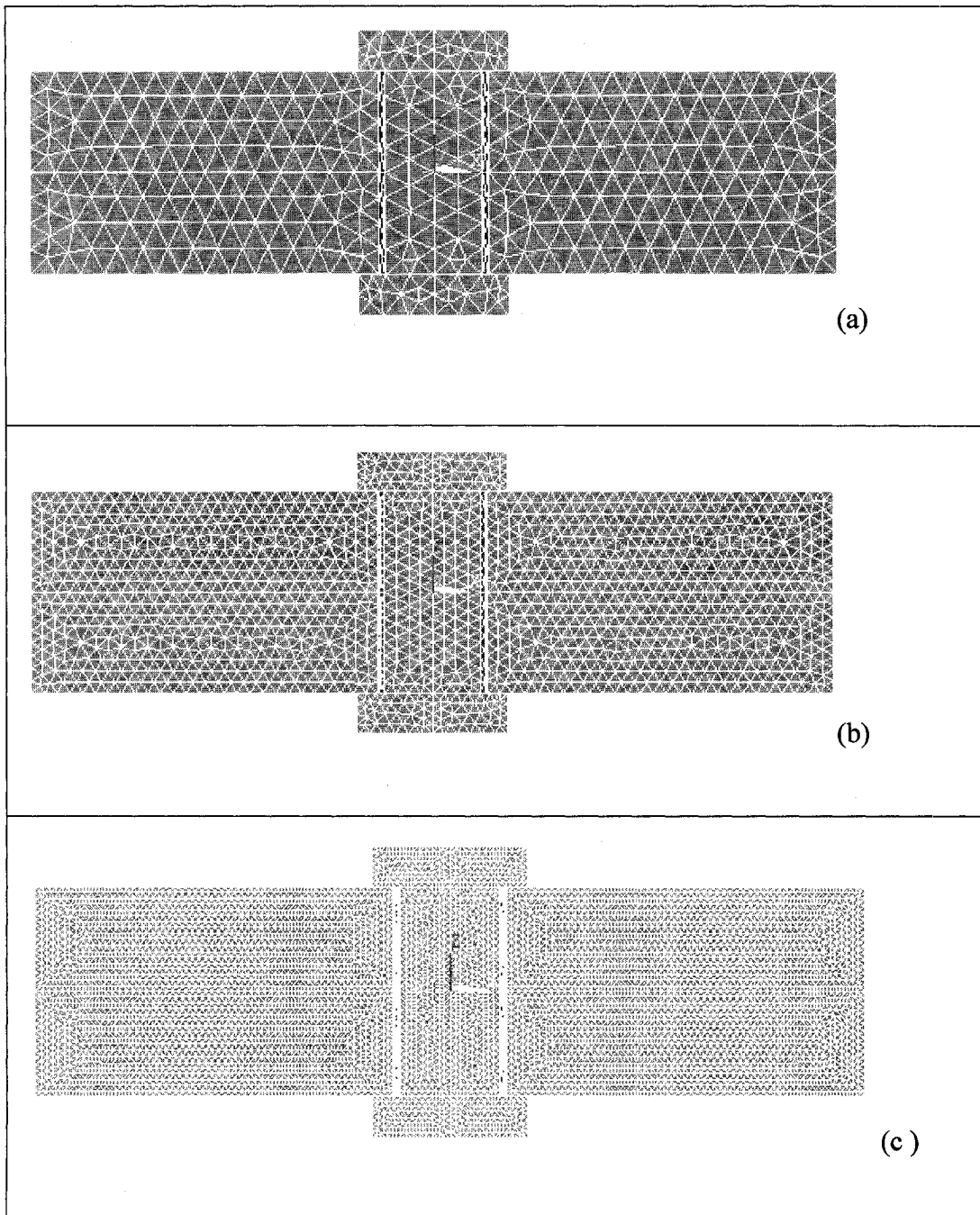


Figure 3.3 Different Density of Mesh Used for Convergence Study

(a) Mesh size 0.0064 (m)(b) Mesh size 0.0032 (m)(c) Mesh size 0.0016 (m)

Table 3.3 Convergence Criteria for Each Mesh Density

Mesh size (m)	0.0064	0.0032	0.0016
Maximum Von Mises Stress (Pa)	$0.71 \times 10^7$	$0.345 \times 10^8$	$0.481 \times 10^8$

The following interactions are modeled:

- Between bolt head and member interface
- Between bolt nut and member interface
- Between two members.

Contact is defined through surface-to-surface contact elements. TARGE170 is used to represent surfaces for the associated CONTA174 elements. These target elements overlay the solid elements describing the boundary of the deformable target body. There is no initial penetration before applying pretension.

TARGET170 is used to represent various 3 dimensional surfaces associate with different contact elements, such as CONTACT174. The contact elements overlay the elements on the boundary of the body which are in contact with the target elements. The target surface is modeled through different target elements, each target surface is consisting of several target elements.

Contact occurs when the element surface penetrates one of the target segment elements on a specified target surface. Coulomb and shear stress friction is allowed. The CONTACT 174 is defined by eight nodes. The 3-D contact surface elements are associated with the 3-D target segment elements via a shared real constant set. Figure 3.4 shows the schematic contact between each target 170 and CONTACT 174 element.

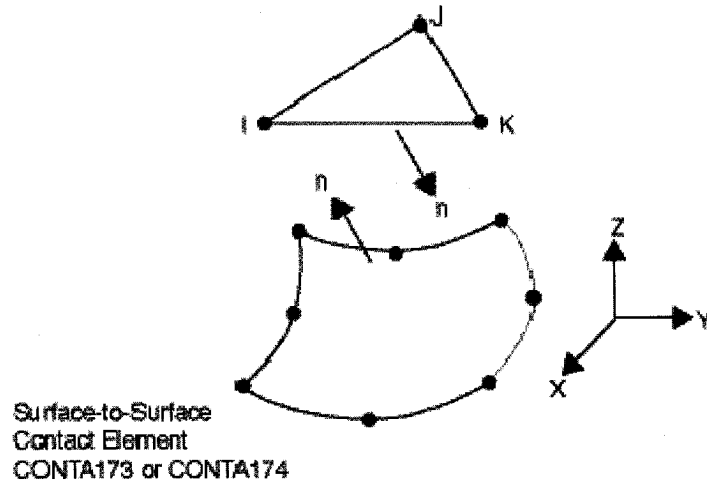


Figure 3.4 TARGET170 Geometry [ANSYS (2003)]

### 3.3 Finite Element Results

Figure 3.5 shows the counter plot of the resultant von Mises stress after applying the pretension to the connection. The plot clearly represents that the stress is distributed in the frustum region around the bolt hole.

To calculate the stiffness from the simulations, the elements at the interface of the bolt head-nut with the member could be placed in a set; therefore by dividing the force over the average relative displacement of these two sets, the stiffness can be calculated and used for comparison.

The calculated member deformation at the bolt head and the member interface is  $1.069 \times 10^{-6} \text{ mm}$ . The calculated member stiffness, according to the equations 3.1 and 3.2, is  $4.944 \times 10^9 \text{ N/m}$ .

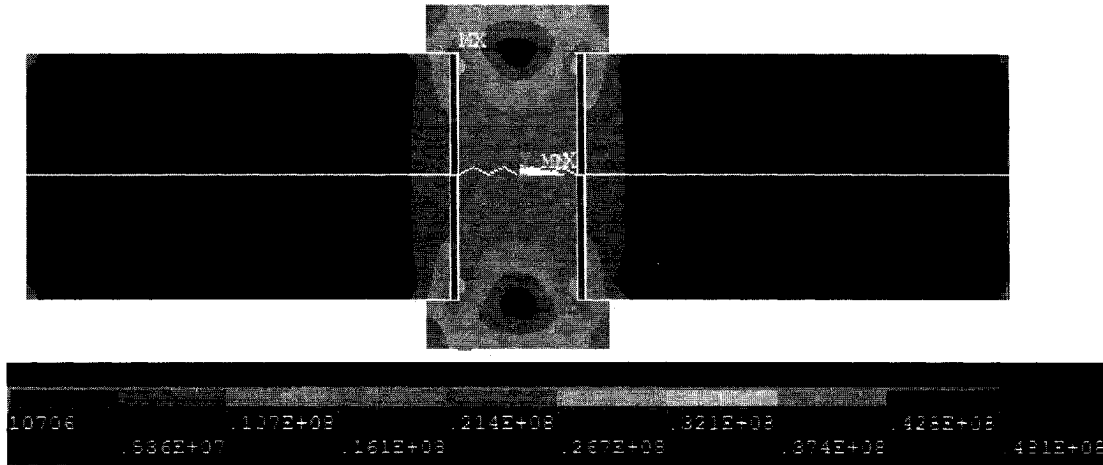


Figure 3.5 Von Misses Stress (Pa) Distributions in the Frustum Zone Around the Bolt Hole

$$Stiffness = \frac{Applied\ Load}{Average\ Member\ Deflection} \quad (3.1)$$

$$K_m = \frac{10572N}{1.069 \times 10^{-6} \times 2m} = 4.944 \times 10^9 N/m \quad (3.2)$$

To investigate the accuracy of the results achieved from this study, they are compared with other sources. The comparison displayed in the table 3.4. The method for calculating the stiffness for each theory is described in Appendix A. The reason for the differences between these studies will be discussed in a later section.

Table 3.4 Comparison of the Joint Stiffness Calculated in Different Studies

Different Studies	Results
Three Dimensional Finite Element Analysis (Thesis)	$4.944 \times 10^9 N/m$
Experimental Result by Maruyama et.al (1975)	$5.11 \times 10^9 N/m$
Shigley and Mischke (1995)	$5.9 \times 10^9 N/m$
Wileman et.al (1991)	$5.57 \times 10^9 N/m$
Lenhoff et.al (1994)	$5.775 \times 10^9 N/m$



### 3.4 Energy Balance Study of the Model

Evaluating the preloaded joint versus deflection curves provides insight to the strain energy method. The slope of the curves represents the stiffness of the bolt members as shown in figure 3.6. The areas projected under these curves, represent the stored strain energy in the bolt and members.

The member and bolt stiffness are calculated as in equations 3.3 and 3.4.

$$K_b = F_i / \delta_b \quad (3.3)$$

$$K_m = F_i / \delta_m \quad (3.4)$$

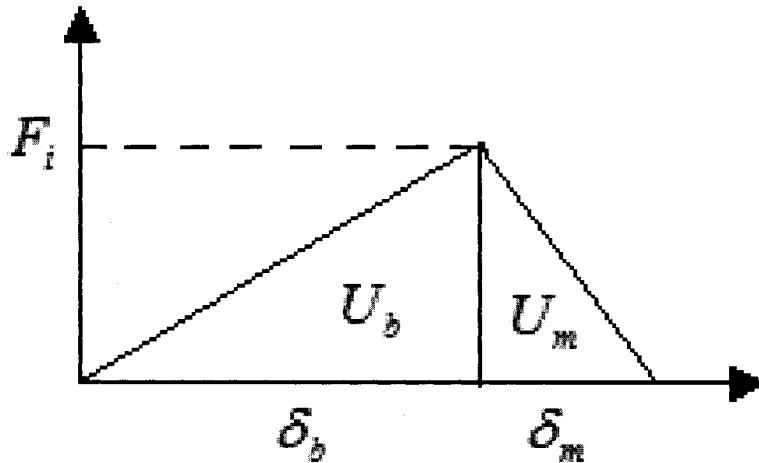


Figure 3.6 Strain Energy Driven from the Force-Displacement Curve [Allen 2003]

According to equations 3.5 and 3.6, the strain energy is equal to the area under the force displacement curves.

$$U_b = F_i \times \delta_b / 2 \quad (3.5)$$

$$U_m = F_i \times \delta_m / 2 \quad (3.6)$$

$U_b$  and  $U_m$  are the strain energies of the bolt and the members.

Therefore, the stiffness of bolt and member can be rewritten in terms of the strain energy, according to the equations 3.7 and 3.8.

$$K_b = F_i^2 / 2U_b \quad (3.7)$$

$$K_m = F_i^2 / 2U_m \quad (3.8)$$

Since only the pretension is applied to the structure, the relation between the strain energy, the stiffness of bolt, and members, is defined as in equation 3.9.

$$\frac{U_b}{U_m} = \frac{K_m}{K_b} \quad (3.9)$$

All the values in this equation can be recorded from finite element analysis and are summarized in table 3.5. Stiffness values are calculated by measuring the displacements. The strain energy values are also derived from the results. An element table is defined for calculating the strain energy values for each element. The values of each element table are added together to get the total strain energy of each part.

Table 3.5 The Strain Energy and Stiffness for Each Part of the Connection

	Bolt	Member
Strain energy	<i>0.0384 Nm</i>	<i>0.0113 Nm</i>
Stiffness	$1.45 \times 10^9 \text{ N/m}$	$4.944 \times 10^9 \text{ N/m}$

Equation 3.9 works for the measured values of table 3.4. Therefore these values meet the criteria for energy balance.

### 3.5 Effect of Having a Washer in the Resultant Stiffness

In this section, the effect of using the washer on the joint stiffness and the stress distribution will be discussed.

A washer with the thickness of 2 *mm* and with the same radius as the bolt head is modeled. There is a small gap between the washer and the bolt shank. Material of the washer is the same as in other parts of the connection.

The length of the bolt shank in this model is 4 *mm* longer than the one in the previous problem, which is negligible compared to the total length of 54 *mm*. The member geometries are exactly the same as that of the problem discussed in the previous section.

The model is meshed with SOLID185 elements. The element size is chosen as the same size used in the previous problem. Contact is defined between the following regions:

- Bolt head-nut and the washers
- Members and the washers
- Two members

The schematic model is shown in figure (3.7).

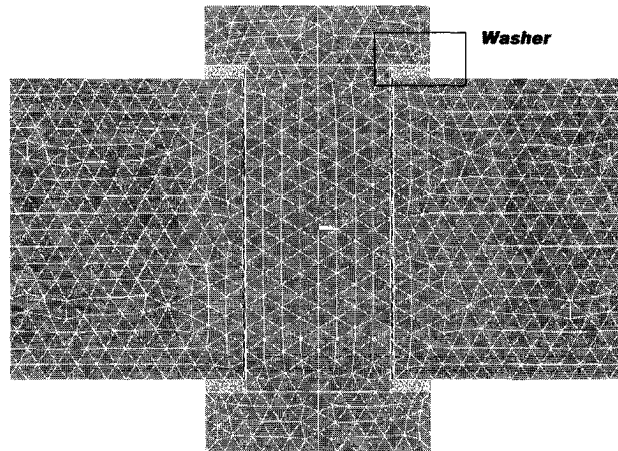


Figure 3.7 Schematic Model of the Joint with Washer

By measuring the displacement, we can derive the stiffness of the bolt and members. Member stiffness of the problem is calculated as  $4.94 \times 10^9 \text{ N/m}$ , which is very close to the value calculated in the previous problem.

The stress distribution of the connection is shown in figure (3.8). According to this figure, the stress is distributed uniformly in the members.

Regarding these observations, we can see that the washers have no significant influence on the deformations and the member's stiffness. The washers generally contribute to the localization effect of the compressive load only.

The two most common purposes of using washers are:

- To distribute the pressure of the nut or bolt head evenly over the parts,
- To provide a smooth surface and to prevent the loss of preloading as a result of an uneven fastening surface.

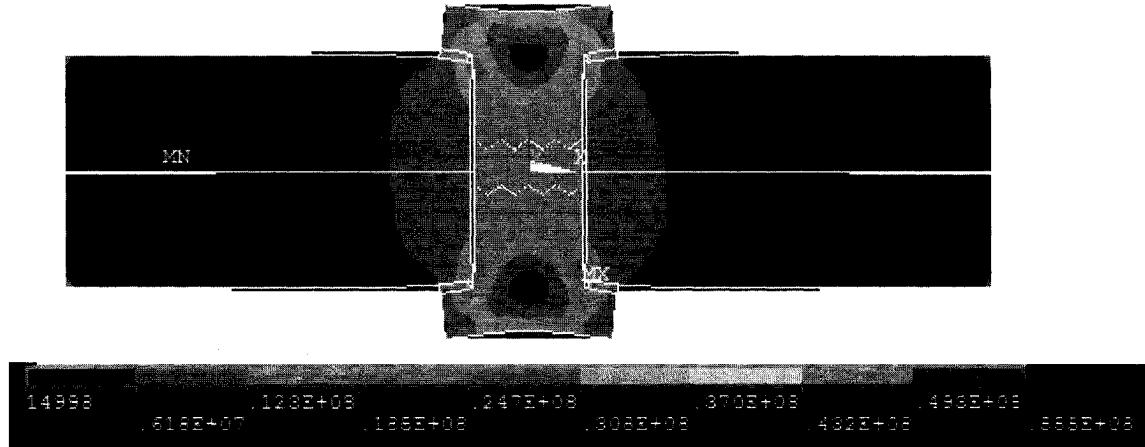


Figure 3.8 Stress Distributions (Pa) in Presence of Washer

### 3.6 Discussion of the Results

The differences between the results of this study and the previous investigation for calculating the stiffness of a classic joint are compared. The results show that the stiffness from the previous investigations is higher than the one calculated in this study and three dimensional analysis results are closer to the results from the experimental investigation.

The reason that Wileman et al results yielded higher values for stiffness is that they used the stiff washer, which caused a uniform displacement at the member surfaces. However an actual washer may be deformed differently when the joint is loaded. By modeling the stiff washer Wileman et al could not represent the effect of bolt's head and its influence on the member stiffness.

On the other hand, the symmetry is not an exact representation of the behavior of a real joint. In real problem the members could be separated, while the separation will affect the changes in stiffness values.

The stiffness calculated by Shigley's theory, did not consider any separation in the contact area or bending at the interfaces, which is the reason for having a higher stiffness value result.

Lenhoff et. al considered the effect of bolt head on the members and also considered the contact in the interface by modeling both the bolt and the members. The reason for the difference between their results and the experimental results is that, they performed their study for a certain range of values, which could not give the exact value for a specific joint.

According to these observations and discussions, the three dimensional model of the mentioned joint seems to be more accurate. It overcomes the overestimation of the previous studies by modeling all bolt parts and representing the actual contacts between the parts.

The reason that the results from this study yields a relatively smaller stiffness value compared to the experimental results is that the bolt shank's diameter is smaller than the bolt hole.

The effect of washer on the stress and the stiffness of the member is also studied. The results show that washers do not have a significant influence on the deformations and the member's stiffness. The washers generally contribute to a localization effect of the compressive load only.

**CHAPTER FOUR**  
**INVESTIGATING ZHANG'S THEORY BY SIMULATING AN**  
**AXISYMMETRIC LOADED JOINT**

In this chapter, an axisymmetric model with an axisymmetric external load is studied to validate Zhang's model. The model that was discussed in the previous chapter is considered in this chapter; however an external force is applied to the model in addition to the pretension force. Because there is no experimental model, which we can correlate with our results, we will check the accuracy of model by considering the load location factor.

As will be discussed later, the load location factor should have specific values for each arbitrary joint. The accuracy of our model is determined if the load location factors of this model, calculating from Zhang's theory, matches the expected values.

#### **4.1 Load Location (Plane) Factor Definition**

The load location factor is introduced in *VDI 2230* (1986). The bolt load is substantially lower than the one predicted by equation 4.1. According to the equation 4.1, the bolt load is dependent on the load factor, while the load factor will be different when changing the location of external load.

$$F_b = F_i + CF \quad (4.1)$$

The load factor  $C$ , derived from the equation 4.2, is valid when the external load is applied directly at the bolt head. In other cases, only a fraction  $n$  of the load factor is effective according to equation 4.3. The physical explanation for the load location factor is that the external load is applied at some point in the middle of the members as describes in figure 4.1.

$$C = \frac{K_m}{K_m + K_b} \quad (4.2)$$

$$n = \frac{C_n}{C} \quad \text{or} \quad n = \frac{F_1}{F} \quad (4.3)$$

Where  $C_n$  is the load factor for an arbitrary location of the external load.

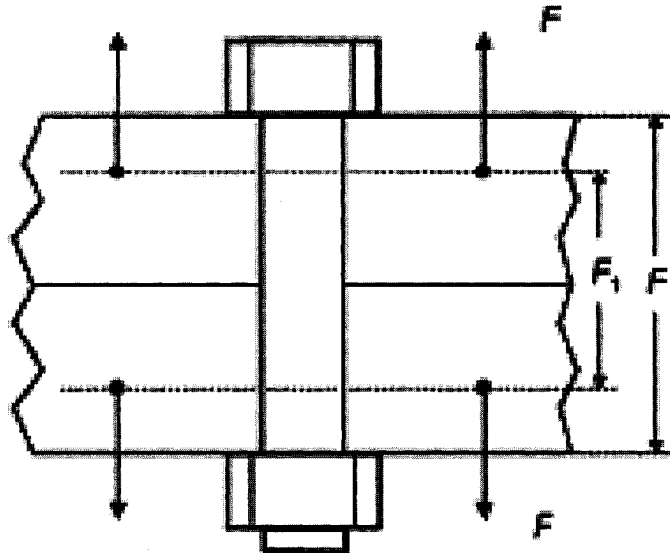


Figure 4.1. Load Location Factor [NTST (1998)]

The recommended numbers for  $n$  are indicated by VDI. The suggested values are: 1 at the bolt interface, 0.5 at the middle of each member, and 0 at the members interface.

The calculated values for  $n$  from our study will be compared to the indicated values from VDI. If these two values are correlated, the accuracy of our model is validated.



## 4.2 Finite Element Model Description

The connection simulated, is similar as the one discussed in the previous chapter, with the same geometry and material; however an axisymmetric load is considered.

The top and the bottom members have the same thicknesses. The effect of contact between the members is considered. Bolt head, nut, and shank are modeled to create more a realistic joint.

PLANE42 [ANSYS (2003)] with two degrees of freedom is used for modeling two-dimensional asymmetric structures. Due to the possibility of bending in joint members, the first order element is used to avoid shear locking. Linear isotropic material is used for both bolt and members.

Contact elements are defined between the following three interfaces in which sliding or separation may occur:

- The surfaces between the bolt head and the top member
- Between bolt nut and the bottom surface, and finally
- The surface between the top and bottom members

The pretension is applied through the pretension element by applying a constant force equal to  $10.566 \text{ kN}$ . This value is twice the preload value that was used in the previous chapter due to the symmetry.

External load, equal to  $5 \text{ kN}$ , is applied to nine different points. The locations of the applied external loads are given in table 4.1 and are shown in figure 4.2.

Table 4.1 Locations of the Applied External Load

Location	Point1	Point2	Point3	Point4	Point5	Point6	Point7	Point8	Point9
X (m)	0.0145	0.0145	0.0145	0.0215	0.0215	0.0215	0.032	0.0325	0.0325
Y (m)	0.024	0.012	0.001	0.024	0.012	0.001	0.024	0.012	0.001

Ten different analyses have been carried out. In the first analysis, pretension is applied. The result is compared with the result of a three-dimensional analysis, which was discussed in chapter three. Then the external load is applied to the preloaded connection in the other nine analyses. The load is applied in nine different positions to study the effect of the applied load location of the bolt load.

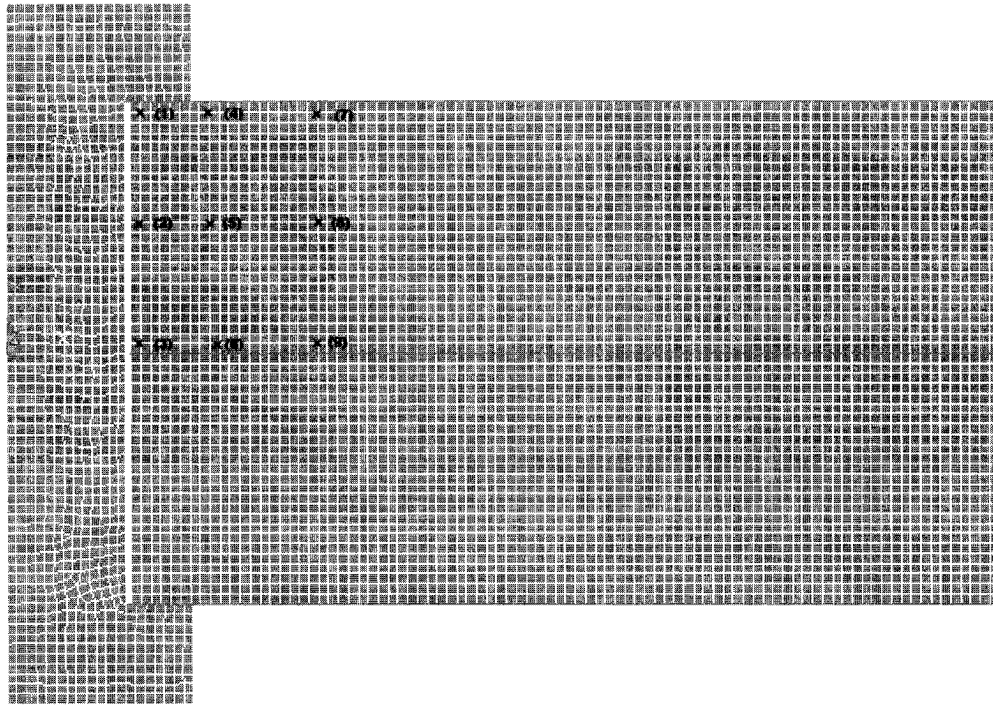


Figure 4.2 Different Locations of the Applied External Load

### 4.3 Finite Element Results

The result from the first analysis is compared with the three-dimensional analysis of the previous chapter. Both analyses incorporate the frictionless contact with linear material properties. Table 4.2 compares the results from both analyses. Since the results are very close, the axisymmetric simulation is used for the rest of the study.

The bolt and member deformations are measured at the center of the interface between the bolt head and the member (Point A shown in figure 4.3). The member stiffness is obtained through the member displacement.

$$K_m = -F_i / \delta_{m,F_i} \times 2 = 10.566 \text{KN} / 1.054 \times 10^{-6} \text{m} \times 2 = 5.01 \times 10^9 \text{ N/m} \quad (4.4)$$

Figure 4.3 shows the stress distribution in bolt and member when only the pretension is applied to the connection. The frustum zone is clearly noticeable in the members.



Figure 4.3 The von Mises Stress (Pa) Distribution in the Frustum Zone Around the Bolt Hole

Table 4.2 Joint Stiffness Values of 2D and 3D Analysis

	<b>Member Stiffness</b>
Two Dimensional Analysis	$5.01 \times 10^9 \text{ N/m}$
Three Dimensional Analysis (Chapter Three)	$4.94 \times 10^9 \text{ N/m}$

#### 4.4 Calculating the Loading Plane Factor using the Zhang's Method

Applying external load will change stiffness of the joint and the load factor. For this, we would like to investigate the effect of external load on the calculation of the member stiffness. New analytical method is used for calculating the member stiffness.

The external load is applied in different locations. In order to calculate the stiffness and the load factor, we need to calculate the additional displacements for calculating the Zhang's model factors. The measured displacements at different locations are given in table 4.3

Table 4.3 Different Deformation Measured from FEA

	$\delta_b \times 10^{-6}$ (mm)	$\delta_m \times 10^{-6}$ (mm)	$\delta_{m,F} \times 10^{-6}$ (mm)	$\delta_\theta \times 10^{-6}$ (mm)
Point1	7591	4253	3627	2.5
Point2	7306	4194	1408	3.5
Point3	7252	4091	4293	7.5
Point4	7046	4268	5177	14
Point5	6907	4216	3372	22
Point6	6546	4100	734	36
Point7	6777	4273	966	41
Point8	6507	4106	891	55
Point9	6315	4084	794	60

By having the recorded displacements, and cylinder stiffness, Zhang's model factors could be calculated.

$K_c$  is the stiffness of the cylinder under the effective compression load. According to the equations 1.15, the member cylinder stiffness of this joint is calculated in equation 4.5.

$$K_c = \pi(d_s^2 - d_w^2)E/8t = 3.14 \times [(0.0375)^2 - (0.025)^2] \times (206.8 \times 10^9) / 8 \times 0.025 = 2.5365 \times 10^9 \text{ N/m} \quad (4.5)$$

The varying member stiffness, proportional factor, and the rotational stiffness of different locations previously defined by equations 1.17, 1.14 and 1.16 are calculated and summarized in table 4.4.

Table 4.4 Different Factors of Zhang's Model

	$K_b \times 10^6$ <i>N/mm</i>	$K_m(F)$ <i>N/mm</i>	<i>a</i>	$K_\theta \times 10^6$ <i>N/mm</i>
Point 1	1.473	0.0253	43.3	6000
Point 2	1.488	0.0516	13.226	4200
Point 3	1.497	0.749	2.9	2000
Point 4	1.437	0.802	0.838	1070
Point 5	1.467	0.95	0.72	681
Point 6	1.45	1.268	0.12	416
Point 7	1.493	1.296	0.16	365
Point 8	1.458	1.506	0.147	272
Point 9	1.471	1.812	0.131	250

The load factor is calculated from the equation 4.6. The coefficients of  $A(F)$  and  $B(F)$  are calculated according to the equations 1.19 and 1.20.

$$C(F) = (F_b - F_i) / F = [A(F) - 1]F_i / F + B(F) \quad (4.6)$$

The load location factor is calculated relative to the load factor value at point one. The calculated load factors and load location factors for each point are summarized in Table 4.5. According to table 4.5, the load location factors at point 1, 2, 3 are very close to the predicted VDI values (1.0, 0.5, 0.0). VDI estimated the load location factor when the external load is applied at the bolt axis. There are some differences between the values at point 1, 2, 3 with the VDI values. The differences are because the external load is applied along the bolt-member interface. When the location of the external load becomes far from the bolt axis the load location factor is decreased.

According to the Gerbert study [1993] except when the external load is applied close to the washer (Points 1, 2, 4 and 5), the load location factor is less than 0.1. The load location factor always decreases when the point of applying the external load becomes closer to the member interface.

Table 4.5 Load Factor and Load Location Factor at Each Point

	$C_n$	$n$
Point1	0.0695	1
Point2	0.0312	0.457
Point3	0.0058	0.0761
Point4	0.0073	0.512
Point5	0.0055	0.371
Point6	0.0008	0.0518
Point7	0.0015	0.111
Point8	0.0011	0.052
Point9	0.00031	0.009

The accuracy of model is validated by comparing the calculated values for  $n$  and the suggested values in *VDI* and also Gerbert study.

### 4.3. Discussion of the Results

- **The effect of proportional factor to the load location fraction**

The member deformation will be decreased, when the distance between the location of the applied external load and the bolt axis increases. Because the proportion factor has the same behavior as the member deformation behavior, it also decreases when the external load is applied far from the bolt head or bolt axis (Equation 1.16).

Therefore, we can conclude that the proportional factor has the reverse effect as the loading location factor.

- **The effect of rotation stiffness to the load location fraction**

The member rotation increases when the external load is closer to the interface of the members. However, it increases by increasing the distance between the external force and the bolt axis.

The member stiffness has the opposite effect on the member rotation. Therefore the member rotation stiffness will be increased when the location of the external load application is closer to the interface of the bolt head. Therefore, the rotation stiffness has the same behavior as the load location factor.

- **The effect of varying member stiffness on the load factor**

The varying member stiffness, which is caused by applying the external force, is derived from equation 1.20.

Since the varying member stiffness will be increased by increasing the rotation stiffness and decreasing the proportional factor, we can conclude that the member stiffness has the opposite effect compared to the effect of the load location factor.



## CHAPTER FIVE

### NEW ANALYTICAL METHOD FOR STUDYING ECCENTRICALLY LOADED JOINTS

#### 5.1 Introduction

In this chapter, we will investigate the accuracy of the Zhang's model for eccentric loaded joints. In Zhang's model, the member stiffness of axisymmetric bolted joints is calculated analytically.

The fundamental idea of the Zhang's model is that the member stiffness at preload remains unchanged even when the external load is applied. By applying the external force, the joint stiffness can be calculated in terms of the three parameters introduced by Zhang.

For generalizing the Zhang's theory and formulations, for eccentrically loaded joint, we need to show that the initial member stiffness,  $K_m$  of the eccentrically loaded joints, remains unchanged after applying the external load. The stiffness of the joints can also be calculated when the factors of Zhang's model are presented.

T-stubs, which are the most common types of eccentrically loaded joints, are chosen for this study.

#### 5.2. Studying the Behaviour of T-stubs

Figure 1.6 shows different modes of T-stub connection failure. According to the design of the joints, different types of failures might happen. There might be no prying force in the joints that are designed to work under the condition of mode 1. The prying force is transmitted through the members in form of shear forces. The shear force has nothing to do to the preloaded stiffness. However, it causes an additional deformation. These deformations had the same behaviours as the behaviours of the introduced

deformations in the axisymmetric joints, if the Zhang's model could be used for calculating the member stiffness of the joint.

In T-stub connections, the deformation of the joints around the bolt is not symmetric. Because of the eccentric load and the resultant unsymmetrical deformation, the actual distribution of the bolt force does not act on the center of the bolt. As the result of flexural deformations in the flange, the bolt force is acting possibly somewhere between the bolt axis and the edge of the bolt head as indicated in figure 5.1. Prying force always bends the bolt, which increases the stress on one side compared to the other.

When the joint is loaded, the contact pressure will be changed in the interfaces. Contact interfaces will be reduced under the point of the external load application. The presence of bolt prevents the flange from separation. Therefore, the contact area will not be symmetric at different sides of the bolt. These changes of the contact area will be caused by asymmetric rotations on two sides of the bolt.

Because of these asymmetrical behaviours, the average deformations of the joint are used for measuring different displacement values, which are needed in the Zhang's model.

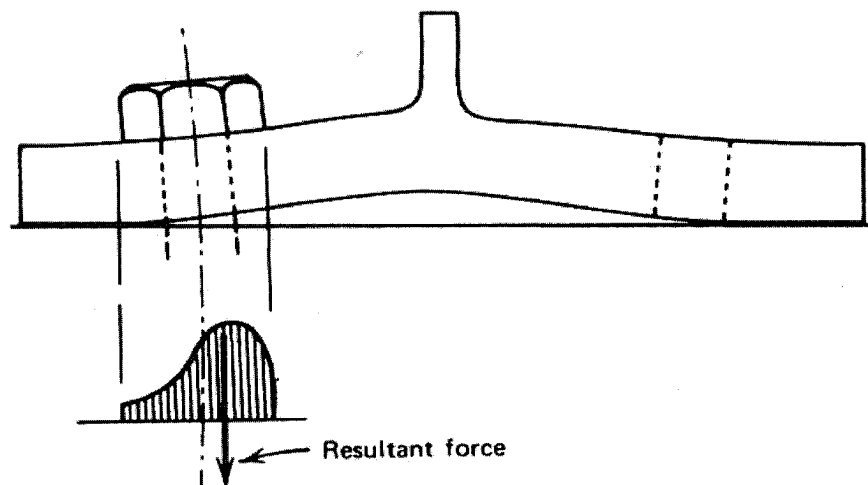


Figure 5.1 Flange Deformation Effect on Resultant Force Location [Kulak et. al (1987)]

The effect of prying action must be reflected for studying the Zhang's model for T-stubs. The theory should contain the effect of this additional force. According to equation

5.1, by increasing the external load  $F$  in the joints, the bolt force  $F_b$  must ultimately resist the full external load plus the full prying force  $Q$ .

$$F_b \geq F + Q \quad (5.1)$$

This equation does not include the preload force. The bolt force will not be equal to the full external load plus prying load at low values of the external load, as long as the preload exists. The bolt will be equal to some portion of the external load or external force plus prying load until the separation of the joints happens.

The introduced factors of Zhang's model are all effective in the T-stubs joint, regardless of whether the prying force appears or not. Only the effect of prying force or preload on these factors is different. The Zhang's theory for joints with prying action needs to include the effect of the prying force. A specific coefficient should also be introduced as prying coefficient.

According to this brief discussion, we can use the Zhang's factors and their related deformations, to study eccentrically loaded joints. In order to study the stiffness of the connection, first we need to know where we can measure these deformations in an eccentric joint.

If the final results from these values and the results from experimental analysis matches, we will be able to prove the accuracy of Zhang's model for T-stubs. To support this theory, a finite element analysis is performed to achieve different displacements of the joint. To correlate the result by a reliable source, the same model as studied by Bursi and Jaspart (1997) will be simulated. The model will be referred to as Bursi's model in the rest of this chapter for convenient.

In the following section, Bursi's model is rerun in the ANSYS software. If the results correlate with Bursi's results, we can use the model for the rest of the study, which is the calculation of the member stiffness according to the Zhang's model.

### 5.3 Model Description

The connection used by Bursi is shown in figure 5.2. The *M12* grade 8.8 bolts and a bolt shank of 21.4 *mm* in length are used, which includes both washer and nut flexibilities. The preloading force of  $F_i = 60.7kN$  was applied and the model is designed to fail according to the mode 1.

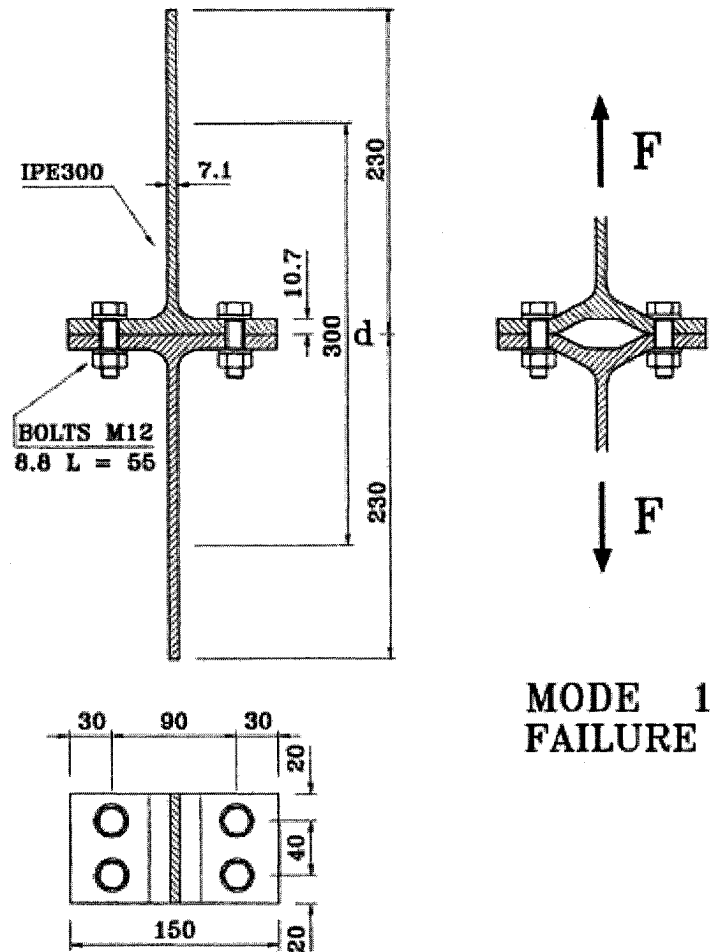


Figure 5.2 Model Geometries in Bursi's Analysis [Bursi and Jaspart (1997)]

In order to perform realistic simulations comparable to the experimental results, actual material properties are used. Therefore, the main material data, values of the yield stress  $f_y$ , the ultimate stress  $f_u$  of the flange, web and bolt materials are reported in table 5.1.

Table 5.1 Material Properties of Each Part Associated with Our Model

T-Stub Parts	Yield Stress (MPa)	Tensile Stress (MPa)
Flange	431	595
Web	469	591
Bolt shank	893	974

#### 5.4 Finite Element Model

Finite element analysis is performed in ANSYS. The complexity of eccentrically loaded joints is significantly greater than the one for centrally loaded joints. The computational requirements of a finite element model of a three-dimensional eccentrically loaded joint compared to an axisymmetric model are much higher. Therefore, we simulate only a quarter of the model's geometry. A rigid foundation is used to represent the lower part of the flange to represent the contact between the two parts and to model the reaction forces. A symmetry plane is used to model the other half of the connection.

The contacts are defined as:

- Between the flange and the base rigid surface
- Between the bolt hole and the bolt shank
- Between the bolt head and the flange surface

No friction has been defined between the bottom flange and the rigid foundation because of the symmetric behavior and the lack of slippage. However, a friction coefficient of  $\mu = 0.25$  has been considered at the bolt head-flange interface.

Two different load steps are performed; in the first load step we apply the pretension, then the external load will be applied in the second load step. Preloading forces are applied through bolt elements (PRETS179). Pretension elements are defined through the pretension section, which is normal to the bolt axis.

The tetrahedral option of the three dimensional-eight-node element, SOLID185, is used to model both bolt and flange. The rigid base is meshed by shell 163 elements with almost the same density of the flange surface. The convergence study has been done to get the best mesh density using three different mesh sizes (1, 2, 4 millimeter) according to figure 5.3. The von Mises stress value selected as the convergence criteria. The values of the von Mises stress are given in table 5.2. According to these values the mesh size of two millimeters is the best case for the modeling. The von Mises stress will not change further by using a finer mesh density.

Table 5.2 Convergence Criteria for Each Mesh Density

Mesh Size	4mm	2mm	1mm
Maximum von misses stress (MPa)	2242	2680	2679

### 5.5 Correlation of the Model with Bursi's Results

The results from our analysis correlate with Bursi's results. Resultant displacement of the web base versus the external load, and also the resultant bolt load versus external loads are summarized figures 5.4 and 5.5, comparing our results with Bursi's results.

The accuracy of the model is established by studying the correlation of our analysis results with Bursi's results. Therefore, we can use the results of our analysis for another purpose, which is the calculation of the member stiffness, in accordance with Zhang's theory.

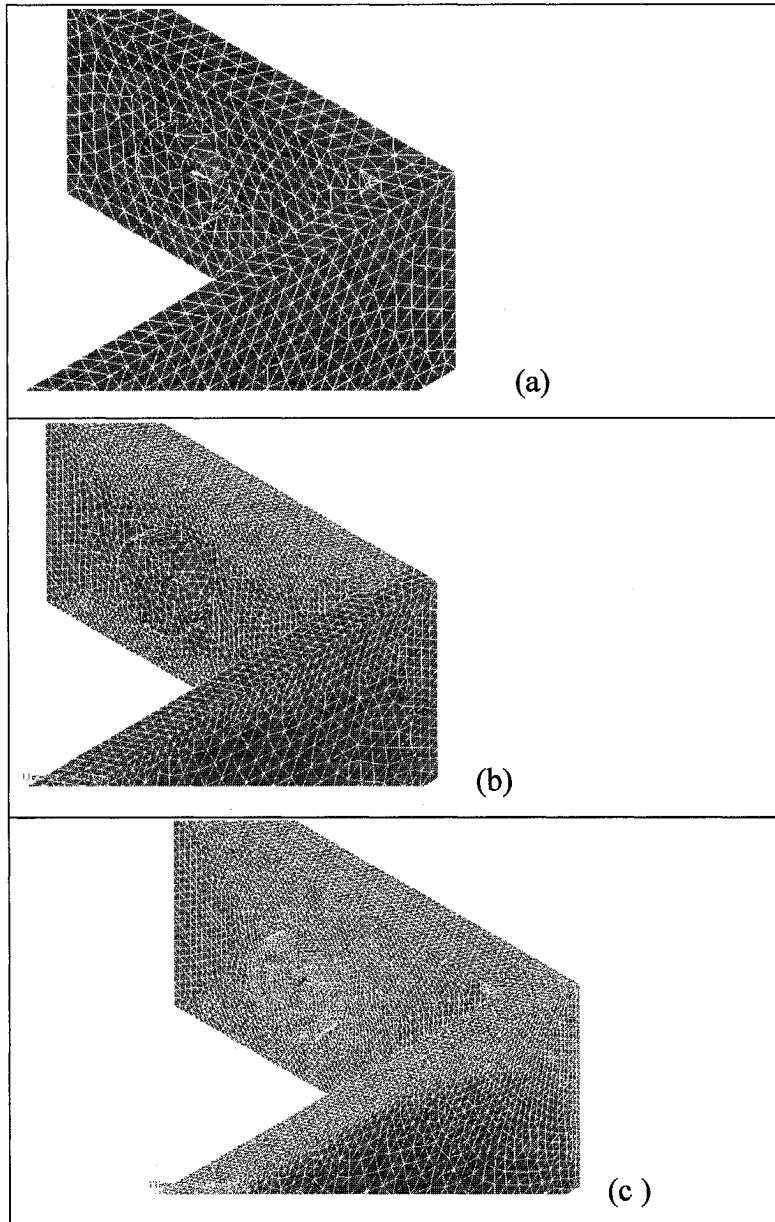


Figure 5.3 Different Density of Mesh Used for Convergence Study (a) Mesh size 4 *mm*

(b) Mesh size 2 *mm* (c) Mesh size 1 *mm*

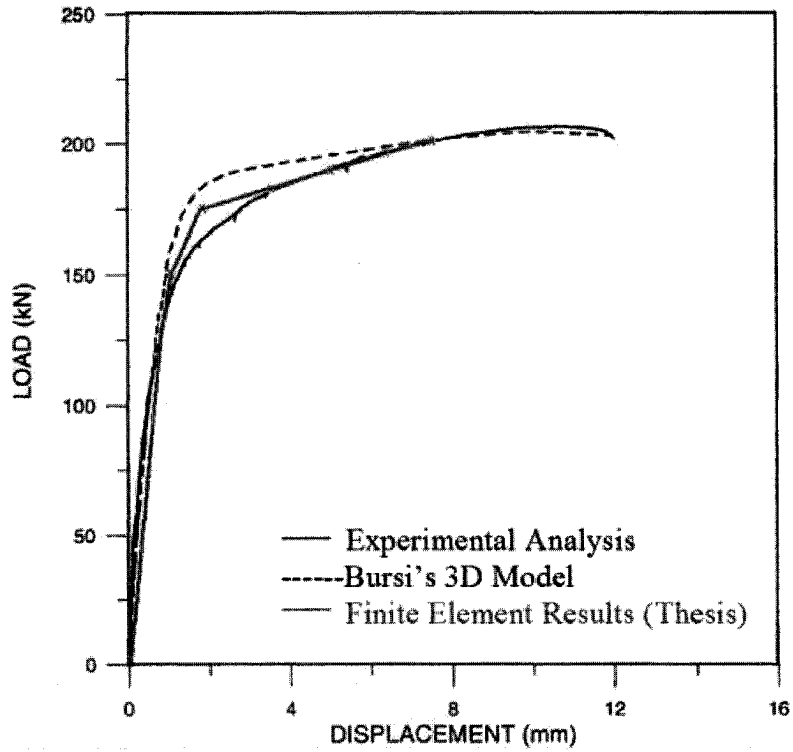


Figure 5.4 External Load vs. Displacement from Finite Element Results and the Previous Study

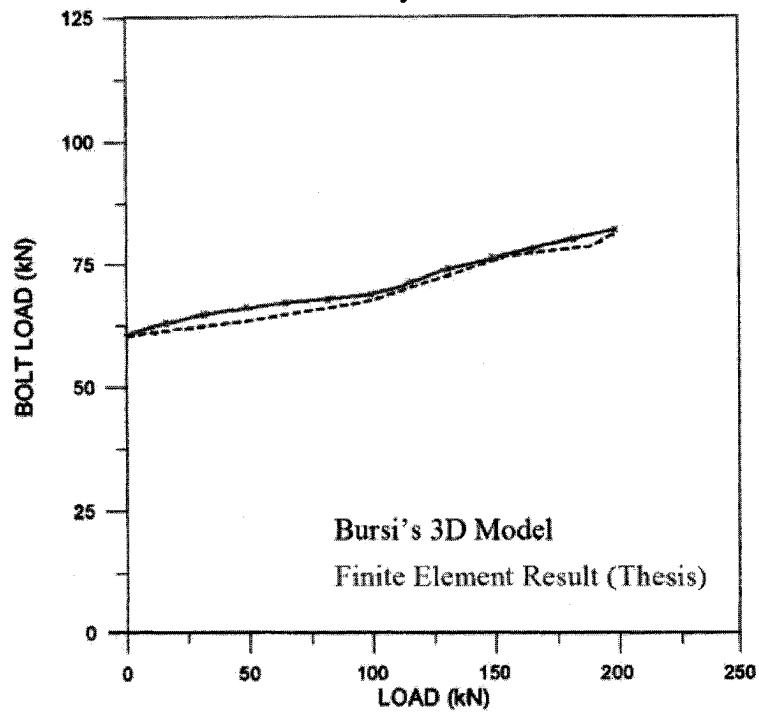


Figure 5.5 External Loads versus Bolt Loads from FE Results and the Previous Study



## 5.6 Analytical Calculation of Member Stiffness According to the Zhang's Model for a Specific Example

After investigating the correlation of the results with the ones from Bursi's, we will proceed for calculating the member stiffness and the bolt load.

### 5.6.1 Member Stiffness Calculation at Preload

First we need to calculate the member stiffness at preload. To correlate the results of the stiffness at preload, we can compare them to the analytical results from the conventional theory. We can assume that the conventional theory could be used for our model, as long as the flange is large enough to include the stress distribution. Since the thickness of the two flanges is the same, we can use the Shigley formula [Shigley and Mischke (1983)] to calculate the stiffness to compare with the finite element results. The bolt and member stiffnesses are calculated according from the bolt and member displacements. The displacements of bolt and members are measured in finite element analysis, which are respectively 0.083 and 0.0217mm.

Figure 5.6 shows the cutting plane area of the model at the centerline of the joints (Section A-A in figure 5.8) to show the stress distribution caused by the pretension, which is a frustum region.

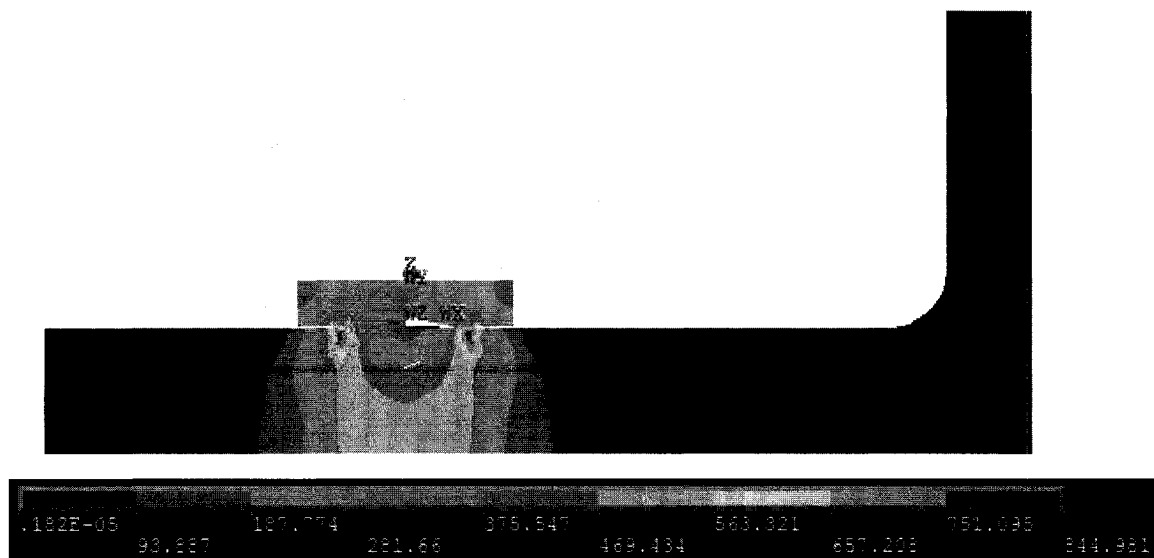


Figure 5.6 The Frustum von Mises Stress (Pa) Distribution Form at the Preload

Figure 5.7 shows the stress distribution on the cutting plane parallel to the flange surface at some arbitrary depth. It is observed that on each arbitrary surface, the stress is distributed symmetrically along the bolt shank's surrounding, which shows the symmetric form of the frustum zone.

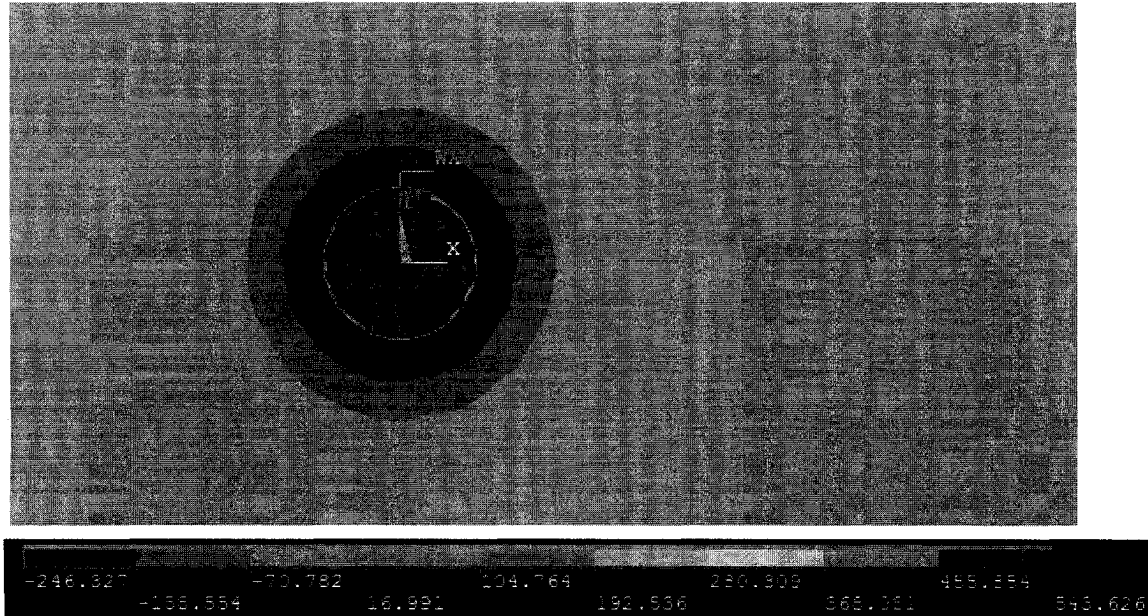


Figure 5.7 Uniform Stress  $\sigma_z$  (Pa) Distributions along the Bolt Hole

Based on the figures 5.6 and 5.7, we can use the conventional theory for calculation of the member stiffness at preload.

The member and bolt stiffness can be calculated in equations 5.2 and 5.3, using the equations (1.3) and (1.13), which were introduced in chapter one

$$K_b = \pi E d^2 / 4(2t + 0.8d) \quad (1.3)$$

$$K_b = 3.14 \times (2 \times 10^5 \text{ N/mm}) \times (12)^2 / 4(2 \times 10.7 + 0.8 \times 12) = 7.29 \times 10^5 \text{ N/mm} \quad (5.2)$$

$$K_m = \frac{\pi E d \tan \alpha}{2 \ln \left[ 5 \frac{2t \tan \alpha + 0.5d}{2t \tan \alpha + 2.5d} \right]} \quad (1.13)$$

$$K_m = \frac{3.14 \times (2 \times 10^5 \text{ N/mm}) \times 12 \times \tan(30^\circ)}{2 \ln \left[ 5 \frac{2 \times 10.7 \times \tan(30^\circ) + 0.5(12)}{2 \times 10.7 \times \tan(30^\circ) + 2.5(12)} \right]} = 28.125 \times 10^5 \text{ N/mm} \quad (5.3)$$

The member and bolt stiffness resulted from this finite element analysis are also calculated from equations (5.4) and (5.5) based on the measured deflection of bolt and member. The calculated stiffness from both methods is given in table 5.3.

$$K_m = \frac{\text{Applied Load}}{\text{Average Member Deflection}} = \frac{60.7\text{KN}}{0.0217\text{mm}} = 27.87 \times 10^5 \text{ N/mm} \quad (5.4)$$

$$K_b = \frac{\text{Applied Load}}{\text{Average Bolt Deflection}} = \frac{60.7\text{KN}}{0.083\text{mm}} = 7.31 \times 10^5 \text{ N/mm} \quad (5.5)$$

Table 5.3 The Bolt and Member Stiffness from the Finite Element Analysis, and Conventional Theory

	$K_b (N/mm)$	$K_{m,F_i} (N/mm)$
Theory (Shigely's Formula)	$7.29 \times 10^5$	$28.125 \times 10^5$
FEA (Thesis)	$7.31 \times 10^5$	$27.87 \times 10^5$

### 5.6.2 Calculation of the Member Stiffness of Externally Loaded Joints

At this point, we would like to calculate the member stiffness and the bolt load using Zhang's model. To investigate the accuracy of the procedure, we will compare the bolt load values calculated in Zhang's theory, with Bursi's results.

First we will explain the procedure for calculating the member stiffness of the joints with the external force of  $40\text{kN}$ . Figure 5.10 shows a different view of the von Mises counter plot of the model.

Figure 5.9.b shows the counter plot of the von Mises stress on the cutting plane (A-A). As we can see in this figure, the stress is accumulated in two different regions, the web base and the bolt hole. According to the stress value of zero at the tip of the flange, there is no prying force presented.

The reason that the left edge of the bolt is not visible in figure 5.8 (b) is that there are only nine colors for observing the counter plot defined in ANSYS. The relative stress

values of these two regions are closer than the other regions. Figure 5.9 depicts other stress component counter plot of the same surface. The boundary of the bolt stress is more recognizable in other stress components plots.

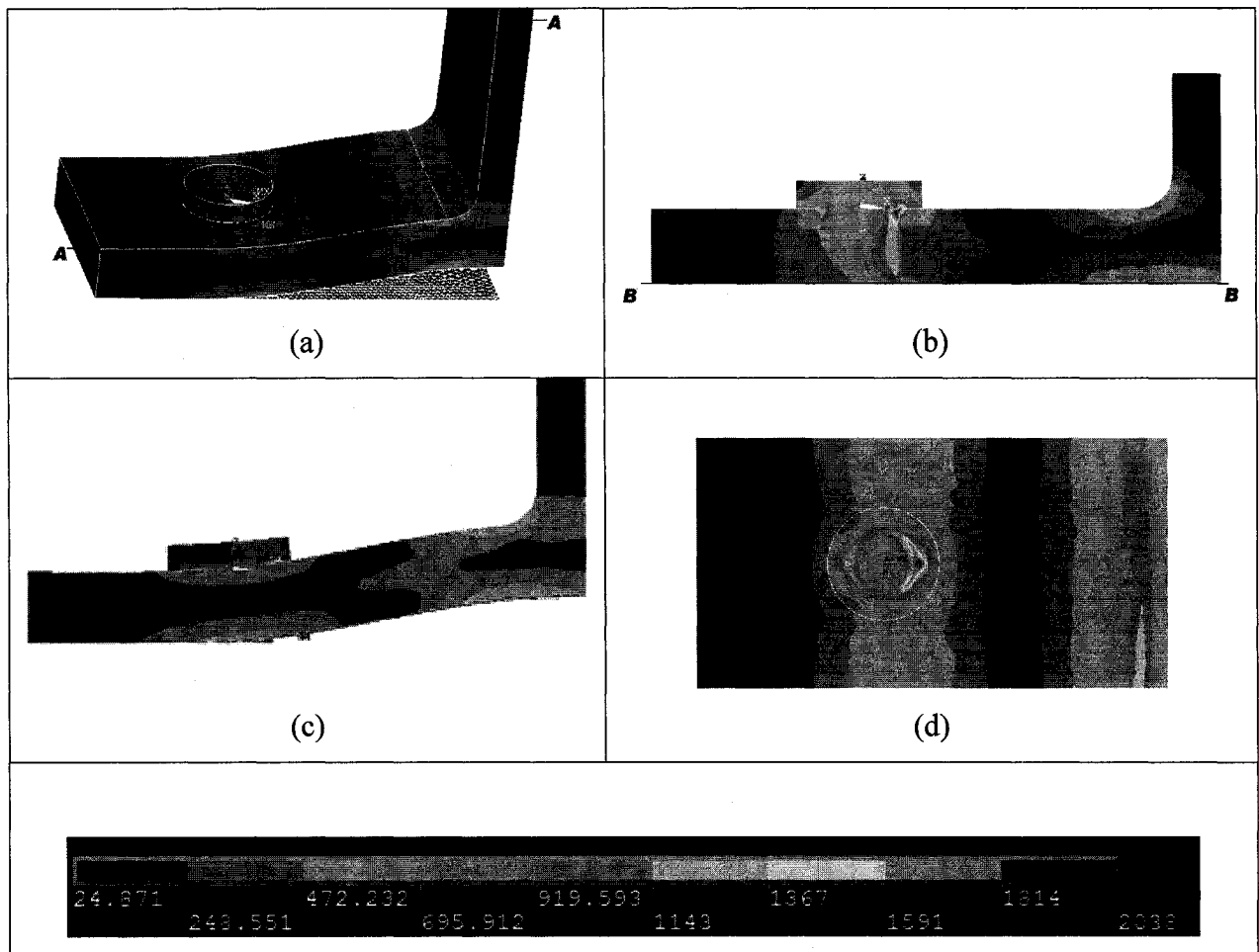


Figure 5.8 Different Views of Von Mises Stress (Pa) Plot of Externally Loaded T-Stub

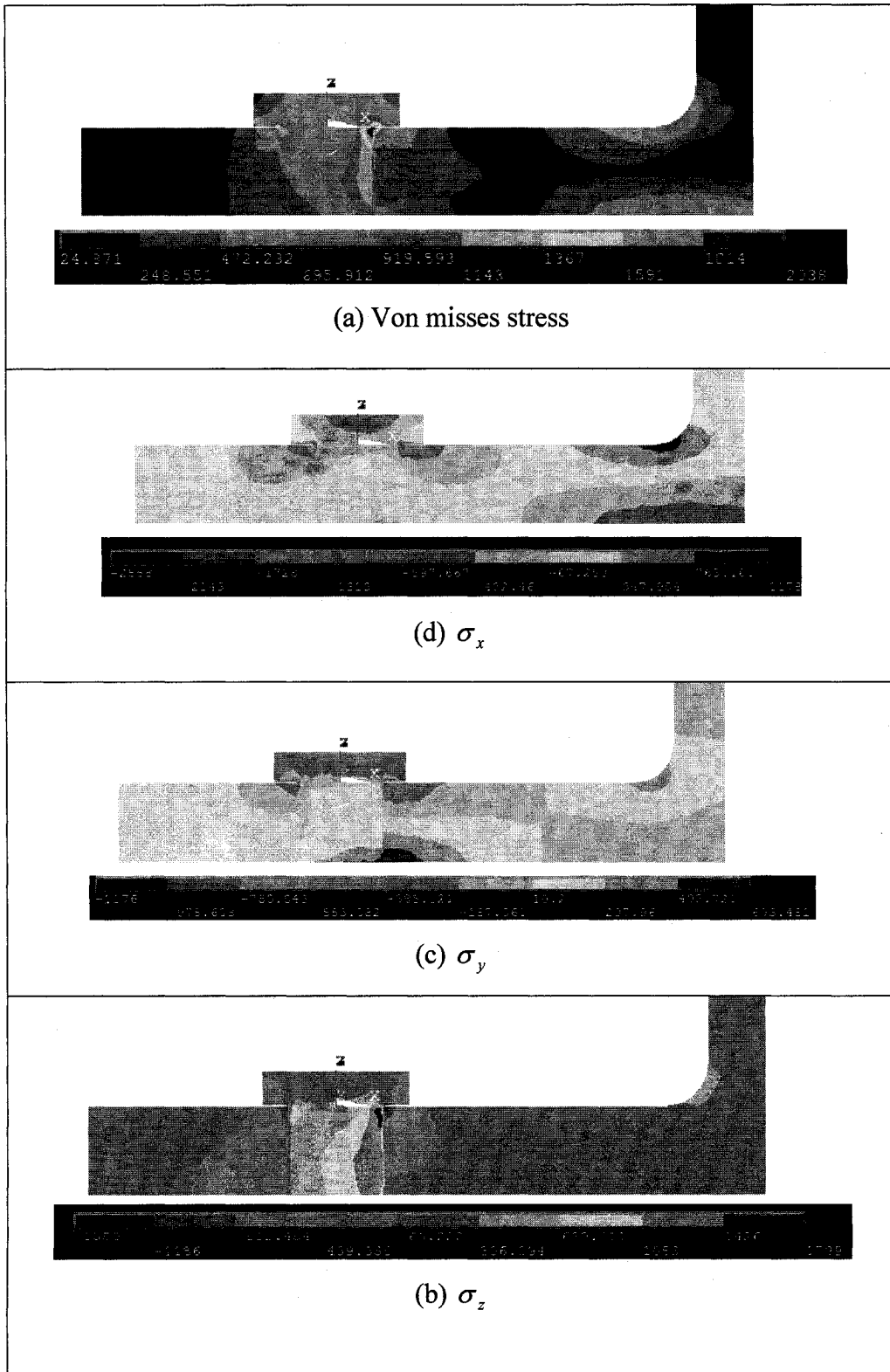


Figure 5.9 Counter Plots of Different Stress Components (Pa)

It should be noted that the joint deformation could not be depicted in the cutting plane plot.

Figure 5.10 shows the displacement of the flange on the defined path from the tip of the flange to the web base (Path B-B in figure 5.8). Vertical axis represents the displacement of the member and the horizontal axis is the geometric coordinate on the path. Units of both axes are millimeter. The picture shows that the deformation of the flange at its interface in the opposite side of the applied external load has even negative displacement. The deformation at the web base has already been matched with the Bursi's results.

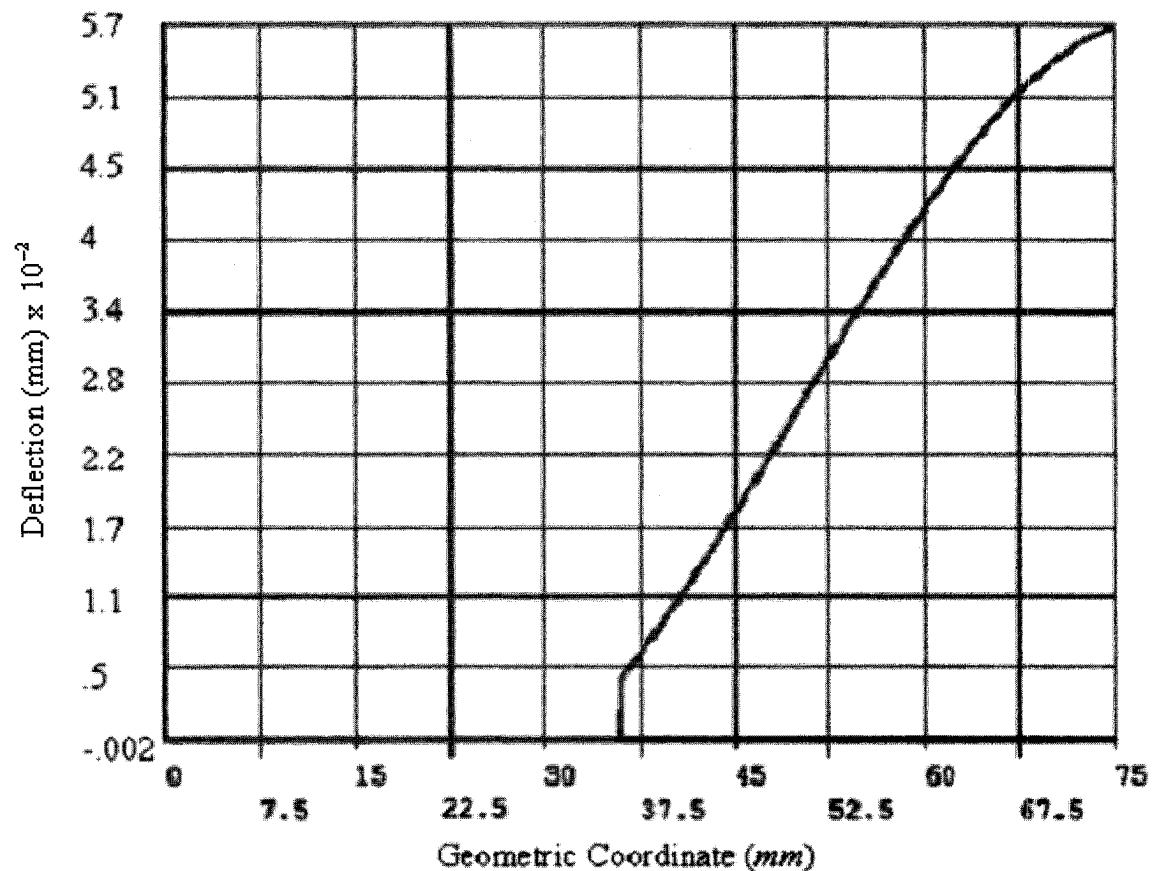


Figure 5.10 The Flange Deformation on the Contact Area of Flange and Base

Unlike the stress distribution at preload, which was symmetric along the bolt hole, the stress distribution is no longer symmetric when the external load is applied. However, we

can show that the behavior of the varying stress is almost the same on each side. To show this, four different paths are defined on four sides of the bolt hole in its depth direction. Von Mises stress is recorded on these paths to confirm this fact (Figure 5.11).

The vertical axes are the von Mises stress and the horizontal axes are the geometric coordinates of the paths.

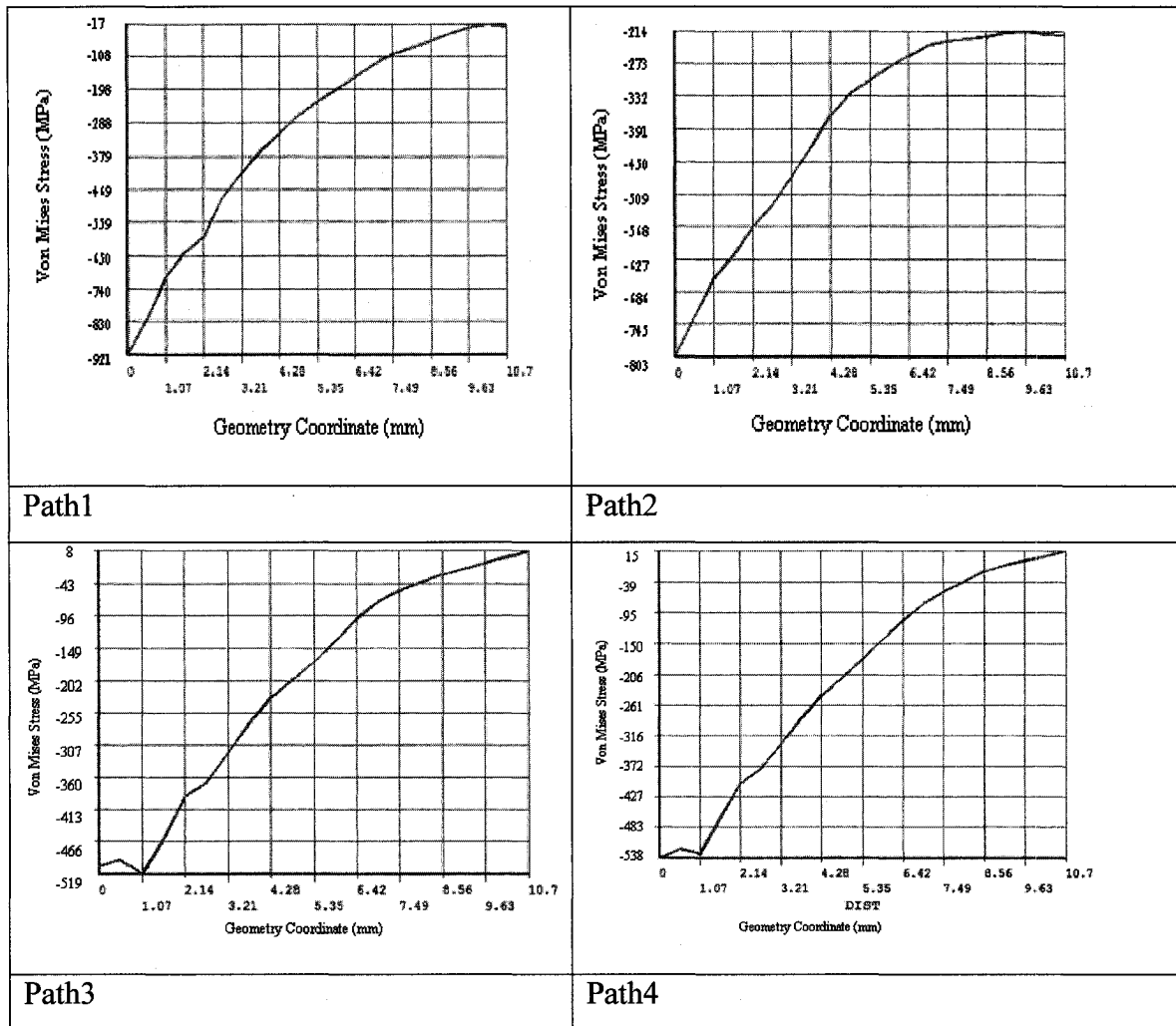


Figure 5.11 The Same Behavior of the Stress Distribution Around the Bolt Plotted are, Von Mises Stress (Pa) vs. Distance (mm)

In order to calculate the joint stiffness, we need to calculate different parameters of Zhang's analytical model. The deformations are caused by the rotation of the joints and

the shrinking of the members in addition to the vertical displacement. Figure 5.12 shows the total deformation and the vertical deformation plots of the joint.

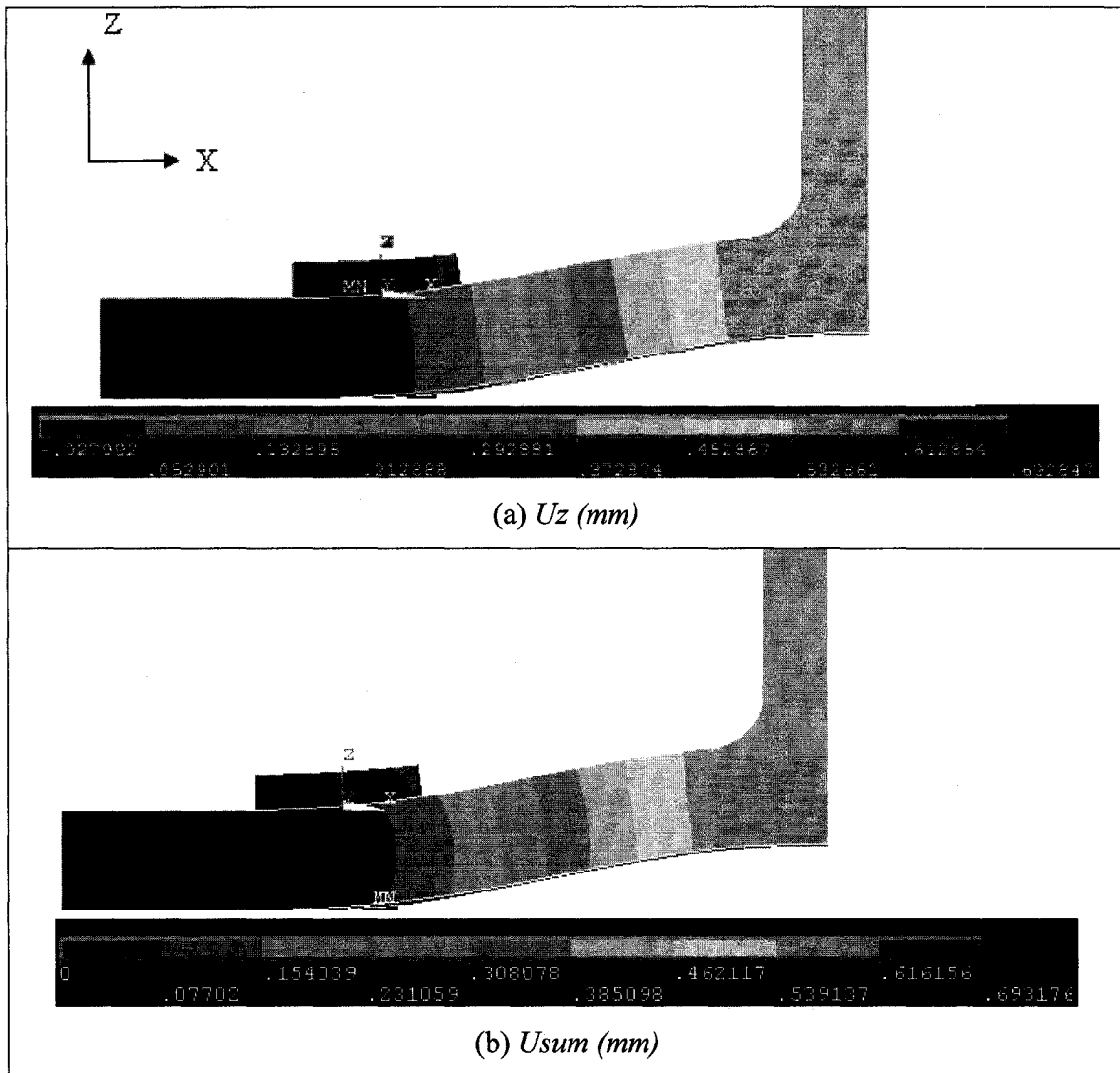


Figure 5.12 The Difference Between the Total and the Vertical Deformation Counter Plot



For calculating the member stiffness we follow these steps:

**(a) Measuring the Displacements**

To read the displacement values, nine different paths are defined according to figure 5.13. The displacement in z direction is mapped into these paths. The values are read before and after the separation. The first four paths plotted are the  $U_z$  along the centerline of the bolt head, and the next four paths  $U_z$  are on the bolt hole interface. Path 9 observes the displacements at the center of the bolt shank.

The final deformations are resulted from the average value on each side of the bolt. Figure 5.14 depicts the position of the defined paths in addition to the method of measuring the axisymmetric model proposed by Zhang's model. The plotted paths for the after separation condition is given in Appendix C as an example. However the recorded displacements are given in table 5.4. The following deflections should be read from the finite element results.

- $\delta_{m,F_i}$  , which is the displacement of the member at preload, measured at the center of the interface between the bolt head and the member, before the separation of the joint.
- $\delta_b$  , which is bolt displacement measured at the same point as  $\delta_{m,F_i}$  .

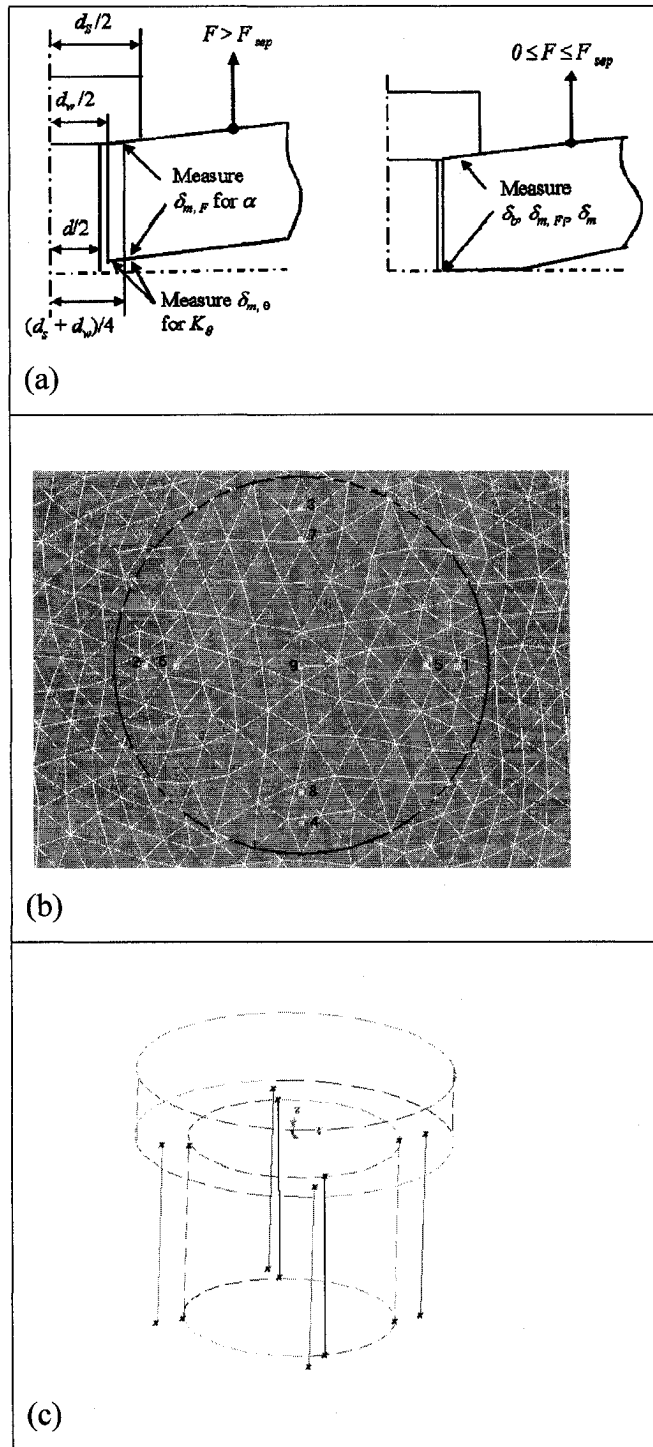


Figure 5.13 The Equivalent Points of Measuring the Displacements (a) The schematic method of measuring the deflections from Zhang's model [Zhang and Poirier (2004)] (b), and (c) The path defined in this thesis for reading the desired deflection values

- $\delta_{m,F}$  , which is the displacement caused by the external load only, which is measured when the joint is separated or without the joint preload. This displacement, caused by compression force, is provided by the external force, which varies through the member thickness.  $\delta_{m,F}$  is determined by measuring the changes in the length of path 1, 2, 3 and 4.
- $\delta_{\theta}$  , which is the joint rotation experienced by the bolt, after separation of the joints. It is measured at the bottom line of each two paths on each side of the bolt.
- $\delta_m$  , which is the total member displacement that is measured before the joint separation. This increase of the deformation is due to the compression caused by external load. Before the separation of the joints, the external load acts as a compression load. As long as the joints are separated the external load will be applied as tensile loading.

The displacement values for the specific applied force of 40 kN are summarized in table 5.4. The average values for each one is given as well. The units for the displacements values are all millimeter.

Table 5.4 The Measured Deformation (*mm*) for Applied Force of 40 kN

	$\delta_b$ mm	$\delta_m$ (Before Separation) mm	$\delta_{m,F}$ mm	$\delta_{m,\theta}$ mm
Side 1	0.04746	-0.001301	0.01330	0.02080
Side 2	-0.002	-0.001313	0.01428	-0.00005
Side 3	0.01327	-0.001289	0.011	0.00244
Side 4	0.01316	-0.001307	0.01107	0.00246
Average	0.01897	-0.013025	0.01241	0.00630

**(b) Calculating the Zhang's Factors**

Zhang's factors are calculated by determining the displacements. Bolt stiffness and cylinder stiffness of the joints should also be computed for these calculations.

The cylinder stiffness is calculated from equation 1.15 as given in equation 5.6

$$K_c = 3.14(18mm^2 - 12mm^2) \times (2 \times 10^5 N/mm) / 8 \times 10.7mm = 13.02 \times 10^5 N/mm \quad (5.6)$$

The external load and prying force, both are transmitted to the effective compression members via shear force. They both produce a reduction in the member thickness. The equivalent reduction from both sources results in  $\delta_{m,F}$ . Proportional factor is calculated in equation 5.7 according to equation 1.14.

$$a = -(13.02 \times 10^5) \times (1241 \times 10^{-5}) / (40 \times 10^3) = 0.403 \quad (5.7)$$

The rotation of the joint is not symmetric along the bolt surroundings. To measure the rotation stiffness, the average rotation is calculated in equation 5.8 according to the equation 1.19

$$K_\theta = (40 \times 10^3) / (63 \times 10^{-4}) \times 2 = 31.7 \times 10^5 N/mm \quad (5.8)$$

When there is no prying force, the residual force is equal to the bolt load minus the external load. Therefore, the varying member stiffness for this connection is calculated according to equation 5.9.

$$K_{m,F} = \frac{(64.1 - 40) \times 10^3}{(1302 - 1241 + 630) \times 10^{-5} \times 2} = 17.43 \times 10^5 N/mm \quad (5.9)$$

The calculated factors are summarized in table 5.5 for further usage in the calculation of the bolt load.

Table 5.5 Calculated Factors of Zhang's Analytical Model

$K_c$	$a = -K_c \delta_{m,F} / F$	$K_\theta = F / \delta_{m,\theta}$	$K_m(F) = F_{res} / ( \delta_m  + \delta_{m,F} + \delta_{m,\theta})$
$13.02 \times 10^5 \text{ N/mm}$	0.403	$31.7 \times 10^5 \text{ N/mm}$	$17.43 \times 10^5 \text{ N/mm}$

(c) **Bolt Load Calculation**

According to the Zhang's analytical method, bolt load is calculated through the equations 5.10 to 5.12.

$$A(F) = \frac{1 + \frac{K_m}{K_b}}{\frac{K_m}{K_m(F)} + \frac{K_m}{K_b}} = \frac{1 + \frac{30.96}{7.25}}{\frac{30.96}{17.43} + \frac{30.96}{7.25}} = 0.87 \quad (5.10)$$

$$B(F) = \frac{1 - \frac{aK_m(F)}{K_c} + \frac{K_m(F)}{K_\theta}}{1 + \frac{K_m(F)}{K_\theta}} = \frac{1 - \frac{0.403 \times 17.43}{13.02} + \frac{17.43}{31.7}}{1 + \frac{17.43}{7.25}} = 0.29 \quad (5.11)$$

$$F_b = A(F)F_i + B(F)F = (0.87 \times 60.7 + 0.29 \times 40) \text{ kN} = 64.409 \text{ kN} \quad (5.12)$$

This calculated value is very close to the calculated bolt force resulted from finite element analysis.

**5.7 Calculating the Joint Stiffness for Different Applied Loading**

The same analysis and calculations were performed for different external forces of 30 kN, 50 kN and 100 kN. The procedure of calculating the bolt load for each applied force is given below:

1. The average measured displacements are calculated and summarized in table 5.6.

Table 5.6 The Average Displacements for Different Applied Loads

	$\delta_b (mm)$	$\delta_{m,F} (mm)$	$\delta_m (mm)$	$\delta_{m,\theta} (mm)$
$F = 30 \text{ kN}$	0.0438	-0.00933	-0.012879	0.00458
$F = 40 \text{ kN}$	0.0442	-0.01241	-0.013025	0.00630
$F = 50 \text{ kN}$	0.03457	-0.01553	-0.01243	0.00779
$F = 100 \text{ kN}$	0.08845	-0.03103	0.02359	0.0299

2. According to the measured displacements, different factors of Zhang's analytical model are calculated and summarized in table 5.7.

Table 5.7 Different Factors Calculated for Different Applied Loads

	$K_b \times 10^5 \text{ N/mm}$	$a$	$K_{m,F} \times 10^5 \text{ N/mm}$	$K_\theta \times 10^5 \text{ N/mm}$
$F = 30 \text{ kN}$	7.246	0.405	18.45	30.89
$F = 40 \text{ kN}$	7.25	0.403	17.43	31.7
$F = 50 \text{ kN}$	7.231	0.4045	16.29	32.06
$F = 100 \text{ kN}$	7.01	0.4041	6.7	33.36

3. For different external loads, the coefficients of the new analytical model of this example are given in table 5.8. As expected,  $A (F)$  is the coefficient of preload and the  $B (F)$  is the coefficient of external load. By increasing the external load, the coefficient of the preload decreases, while the coefficient of the external load increases.

Table 5.8 Coefficients of Preload and Applied Force

	A (F)	B (F)
$F = 30 \text{ kN}$	0.886	0.288
$F = 40 \text{ kN}$	0.87	0.29
$F = 50 \text{ kN}$	0.853	0.308
$F = 100 \text{ kN}$	0.601	0.49

If the joint is designed to have prying force, the effect of prying force should be defined as a new parameter in the equation of the bolt force.

The bolt force value, which is calculated from Zhang's model, overestimates the results from the Bursi's results, when the external load is increased. Because by increasing the external load, the t-stub deformation increases, so does the moment that we neglected in studying the Zhang's model. The moment in the experimental analysis and the finite element model, appears in form of stresses in the model, while the Zhang's model only includes the effects of pretension and external force.

Table 5.9 Comparing the Bolt Load from FEA and the New Analytical Model

	<b>Bolt Load <i>kN</i></b>	
	<b>Finite Element Result (Thesis)</b>	<b>New Analytical Method</b>
<i>F = 30 kN</i>	63.558	62.42
<i>F = 40 kN</i>	64.1	64.4
<i>F = 50 kN</i>	65.289	67.17
<i>F = 100 kN</i>	69.901	73.8

## 5.8 Discussions of the Results

The following conclusions can be made from the analysis described in this chapter:

According to the observation of the finite element analysis, the conventional methods can be calculated for T-stubs if there is no slippage and the flange surface is large enough to include the effective stresses. Therefore, we can use the conventional method formulations for the analytical study.

The behavior of the eccentrically loaded joints can be explained by the factors introduced in Zhang's model.

The bolt load calculation formula introduced in Zhang's model can be used for eccentrically loaded joint if there is no prying force. The additional displacements that are introduced in Zhang's model were all observed in the study of T-stub joint. Therefore, the same factors could be calculated.

According to the design of Bursi's model, the prying force is negligible. Therefore, the bolt load resulted from Zhang's model formula, correlates with the expected results. However, when the prying action is present, the formula introduced in Zhang's model can no longer be used for calculating the bolt force. The bolt force will no longer be a function of the preload and the external load; instead it will be a function of the prying force and the external force. In that situation the bolt load formula will take in the following form:

$$F_b = A(F)Q + B(F)F \quad (5.13)$$



## CHAPTER SIX

### CONCLUSIONS AND RECOMMENDATIONS

#### Conclusions

In this thesis, the analytical solution for calculating the joint stiffness was derived and presented. Three different types of joints were studied and the analytical method was examined for each type, to see the applicability of this method. These three types were consisting of; the symmetric joint with conventional theory assumptions, the axisymmetric loaded joint, and the eccentrically loaded joint.

The main contribution of the thesis is to study the analytical model of the eccentrically loaded joints, which is presented in chapter five. In chapters three and four, the joint stiffness of the conventional and the axisymmetrically loaded joints have been studied through finite element analyses. The functionality and the main concepts of the new analytical model were studied through these benchmarks.

This research has shown that in order to generalize Zhang's model for eccentrically loaded joints, the Zhang's factors should be defined for these kinds of joints as they have been calculated for axisymmetrically loaded and conventional joints.

The theory of conventional joint was clarified in chapter one. In chapter two, different methods, which were used to develop the theory to its final form, were explained. In chapter three, the joint stiffness calculation of a conventional model was studied using finite element analysis and the analytical method. Table 3.4 contains the member stiffness values for a simple conventional joint derived from different studies. According to this table, the best and the most accurate model is derived by eliminating the approximation techniques, such as; using the rigid washers or neglecting the effects of bolt head, nut, and the contact between members.

Furthermore, the effect of utilizing a washer in the connection on the joint stiffness was studied in a separate finite element analysis. The results from this analysis seemed to be very closely matching to the previous results when no washers were used. According to the stress counter plot, washers have no significant influence on the deformations and the member's stiffness however, they generally localize the effect of the compressive load.

According to the table 4.5, the load factor is unity at the first point and decreases as the location of the applied load approaches the member interface. It also decreases when the location of the load moves far from the bolt hole. The behavior and the values of the load factor were within a reasonable range of those in VDI. The agreed results show the accuracy of the analytical model, which has been used to extract this information.

In chapter five, the new analytical model is presented for studying the eccentrically loaded joints. In this new model, three different factors were introduced based on different displacements. The model included the compression force transmitted from the external load and the member rotation experienced by the bolt. The analytical model is formed according to the equations 1.19 to 1.21 and based on  $a$ ,  $K(m)$ , and  $K_\theta$ . The conventional theory is a special application of the new model, however, in conventional theory some of these effects will be neglected. Neglecting these effects, means having the following values in the model:  $K(m) \equiv K_m$ ,  $a = 0$ , and  $K_\theta = \infty$ .

T-stub connection was chosen to represent the eccentrically loaded joint for studying the new analytical model. The Bursi's model was used as an example for the study. The results from this study correlated with Bursi's results.

In order to be able to calculate the member stiffness using the new analytical model, in addition to the member stiffness of joint at preload, different member deformations of the eccentrically loaded joint were needed to be recorded as the data for the analytical model.

According to the table 5.3 and figure 5.6, the conventional method could be used for calculating the member stiffness of the T-stubs at preload. The additional deformations are measured and summarized in table 5.6 for different values of applied load. According to the displacements, the factors of the new analytical model are shown in table 5.7. By having these values, the bolt load can be derived using the equation 1.21. The values of the calculated bolt force, which are derived from the analytical model and finite element analysis, are compared in table 5.9.

The comparison of the values shows that the behaviour of the eccentrically loaded joints can be explained by the factors introduced in Zhang's model. The results also supported the fact that the bolt load calculation formula introduced in Zhang's model can be used for the calculation of the member stiffness for eccentrically loaded joint if there was no prying force.

We can also conclude that the introduced factors of Zhang's model are all applicable in the T-stubs joint, regardless of whether there is prying force or not. When the prying action is presented, the formula introduced in Zhang's model could be no longer used for calculating the bolt force. The bolt force will no longer be a function of the preload and the external load; instead it will be a function of the prying and the external forces. The bolt load formula will then take the following form:

$$F_b = A(F)Q + B(F)F$$

In this case,  $A(F)$  and  $B(F)$  are functions of the prying force and the external load, however, they will still be calculated in terms of the Zhang's model factors and displacements.

## RECOMENDATIONS

According to the discussions in chapter five, the Zhang's model was generalized for studying the member stiffness calculation of eccentrically loaded joints.

The T-stub model, which was used as an example in chapter five, was designed to fail under the first failure mode. According to the model design, the prying action was not presented during the analysis. Therefore, there were no discussions on the bolt load formula developed by applying a prying action.

It is recommended to conduct a series of experimental and analytical analyses for studying the T-stub model that are designed to have prying action. The new bolt load formula based on the prying coefficient can be derived as well.

The Zhang's model did not include the plasticity. Therefore, a new study can be conducted to investigate the possibility of generalizing the Zhang's theory for models with plasticity.

## REFERENCES

Agerskov. H, "Analysis of Bolted Connections Subjected to Prying", *Journal of the Structural Division, American Society of Civil engineering*, Vol. 102(1), 161-75. 1976

Allen. C.T, "Computation of Bolted Joint Stiffness Using Strain Energy", Master of Science Thesis, University of Alabama. 2003

ANSYS Manual Release 8.0 documented. ANSYS Incorporated. Copyright. 2003

Bickford. J.H, "An Introduction to the Design and Behavior of Bolted Joints", 3rd Edition, Marcel Dekker, Inc., New York. 1995

Bursi. O.S, and Jaspart. J.P , "Benchmark for Finite Element Modeling of Bolted Steel Connections", *Journal of Constructional Steel Research* . Vol. 43, Nos. 1-3, pp 17-24. 1997

Bursi. O.S, and Jaspart. J.P, "Basic Issues in the FE Simulation of the Extended End Plate Connections." *Computers and Structures*. 69. 361-382. 1998

Choi. C.K, and Chung. G.T, "Refined Three Dimensional Finite Element for End Plate Connections", *Journal of Structural Engineering*. pp 1307-1316. 1996

Douty. R.T, and McGuire. W, "High Strength Bolted Moment Connections", *Journal of the Structural Division, ASCE*, Vol.91, ST2, 1965

Edward. K.J, and Mackee. R.B. "Areas of Contact and Pressure Distribution in Bolted Joints. ", *ASME Journal of Engineering for Industry*. vol. 94, no.3, pp.864-870. 1972

Gerbert. G and Bastedt. H, “Centrically Loaded Bolt Joints.” *ASME Journal of Mechanical Design*. 115, pp. 701–705. 1993

Gross. I.R, and Mitchell. L.D, “Nonlinear Axial Stiffness Characteristics of Bolted Joints.” *ASME Journal of Mechanical Design*. 122, pp. 442–449. 1990

Highlen. J.L, and Grimm. T.R, “Finite Element Modeling of Bolted Joints”. *Computers in Engineering, San Francisco, ASME*, pp.67-72. 1988

Ito. Y, Toyota. J, and Nagata. S, “Interface Pressure Distribution in a Bolt-flange Assembly” *ASME Journal of Mechanical Design*.. 101-102, pp. 330–337. 1979

Kulak. G, Fisher. J, and Struik. H.A, “Guide to Design Criteria for Bolted and Riveted Joints.” *John Wiley and Sons Inc. Second edition*. 1987

Lehnhoff. T.F, Ko. K.I and Mckay. M.L, “Member Stiffness and Contact Pressure Distribution of Bolted Joints,” *ASME Journal of Mechanical Design*.. 116, pp. 550–557. 1994

Lenhohh. T. F, and Wistehuff. W. E, ”Nonlinear Effects on the Stiffness of Bolted Joints”, *Transaction of the ASME Journal of Pressure Vessel Technology*, vol.118, pp.48-53. 1996

Lim. J, and Nethercot. D.A, “Stiffness Prediction for Bolted Moment Connections Between Cold-Formed Steel Members.”. *Journal of Structures Steel Research* 60. 85-107. 2004

Little. R.E, “Bolted Joint: How Much Give?” *Mechanical Design*. 1967

Maggi. Y.I, Goncalves, R.M, Leon. R.T, and Ribeiro L.F.L, “Parametric Analysis of Steel Bolted End Plates Connections using FE Modeling”. *Journal of Constructural Steel Research* 61, pp. 689-708. 2005

Maruyama. K, Yoshimoto. I and Nakao. Y, “On Spring Constant of Connected Pars in Bolted Joints,”. *Bulletin of the Japanese Society of Mechanical Engineering, JSME*, Vol.18, No.126, pp.1472-1480. 1975

Meyer. G and Strelow. D, “Simple Diagram Aid in Analyzing Forces in Bolted Joints”, *Assembly Engineering*. vol. 15, No. 1, pp.5-33. 1972

Montgomery. J, ”Methods for Modeling Bolts in Bolted Joints.” *Siemens Westinghouse Power Corporation, Orinaldo. (Year not Documented)*

Motosh. N, “Determination of Joint Stiffness in Bolted *Connections*,” ASME J. Ind., 98. pp. 858–861. 1976

NSTS 08307, Revision A, “Criteria for Preloaded Bolts.” *National Aeronautics and Space Administration*. 1998

Osgood. C.C, ”How Elasticity Influences the Bolted Joint *Design*”. *Mechanical Design*. pp 92-95. 1972

Piluso. V.V, Faela. C and Rizzano. G, “Ultimate Behavior of Bolted T-Stubs. I: Theoretical Model”, *Journal of Structural Engineering*, pp 686-693. 2001

Piluso. V.V, Faela. C and Rizzano. G, “Ultimate Behavior of Bolted T-Stubs. II: Model Validation”, *Journal of Structural Engineering*, pp 694-704. 2001

Reid J.D, and Hiser N.R. “Detailed Modeling of Bolted Joints with Slippage”. *Finite Elements in Analysis and Design*, Vol. 41, pp. 547-562. 2005

Rötscher. F, “Die Maschinenelemente“, *Berlin, Springer*. 1927

Sherbourne. A.N, and Bahhari. M.R, “3D Simulation of Bolted Connections to Unstiffened Column-I T-stub Connections”. *Journal of Constructional Steel Research*. Vol.40. No.3 169-187. 1996

Shigley. J.E and Mischke. C.R, “Mechanical Engineering Design,” *6<sup>th</sup> Edition, McGraw-Hill, New York*. 1995

Shigley. J.E and Mitchell. L.D, “Mechanical Engineering Design,” *4<sup>th</sup> Edition, McGraw-Hill, New York*. 1983

Shigley. J.E and Mischke. C.R and Budynas. G “Mechanical Engineering Design,” *7<sup>th</sup> Edition, McGraw-Hill, New York*. 2004

Swanson. J.A, “Characterization of the Strength, Stiffness, and Ductility Behavior of T-stub Connection.”. *PhD Dissertation, Georgia Institute of Technology*, 1999.

Swanson. J.A, Kokan. D.S, and Leon. R.T. “*Advance Finite Element Modeling of Bolted T-stub Connection Components*”. *Journal of Contractual Steel Research*, 58. 1015-1031. 2002

Swanson. J.A, and Leon. R.T. “Stiffness Modeling of the T-stub Connection Component”, *Journal of Structural Engineering*, vol.127, no.5, pp.498-505. 2001

VDI 2230, Verein Deutscher Ingenieure , Part 1, “Systematic Calculation of High Duty Bolted Joints: Joints with One Cylindrical Bolt”, *VDI-Dusseldorf, Germany*. 1986



Wheeler. A.T, Clarke. M.J, and Hancock. J.G. “Finite Element Modeling of Four Bolt Moment End Plates Connections”. *Journal of Structural Engineering*. vol.126 No.7. 2000

Wileman. J ,Choudhury. M and Green. J, “Computation of member stiffness in bolted connections”. *Transaction of the ASME Journal of mechanical Design*, vol. 13, pp. 432-437. 1991

Zhang. O, “ Discussion on Bolted Joints in Tension”, *Transaction of the ASME*, vol.127, pp.506-510. 2005

Zhang. O, and Poirier. J.A, “New Analytical Model of Bolted Joints”. *Journal of Mechanical Design*. vol. 26, pp. 721-728. 2004

## **APPENDIX A - Calculation of the Joint Stiffness from Different Theories for One Specific Problem**

The calculations of the joint stiffness for a specific joint under study using different theories are described in this appendix. The results obtained at this appendix are compared and discussed in chapter three.

### **Experimental Results by Maruyama**

Maruyama performed an axisymmetric finite element analysis of specific connection geometry, including representation of the bolt and nut deflection. He also conducted experimental study using the same geometry. The predicted value for the joint stiffness calculated from the finite element analysis was  $6.29 \times 10^9 N/m$  and the stiffness value calculated by the experimental analysis was  $5.11 \times 10^9 N/m$ . Maruyama's experimental data is useful as a validation for the joint stiffness of this specific model. The following authors used different theories for studying the same model.

### **Shigley**

Shigley simplified the conventional theory using two assumptions. His first assumption was that the compressive load on the member is applied by a washer having the diameter  $d_w = 1.5d$ . He also recommended a value of  $30^\circ$  for the frustum angle. The joint stiffness calculation method for the model discussed in chapter three is given here.

$$K_m = \frac{0.577\pi Ed}{2 \ln \left( 5 \frac{0.577L + 0.5d}{0.577L + 2.5d} \right)} \quad (1.11)$$

$$K_m = \frac{0.577 \times 3.14 \times (206.8 \times 10^9 \text{ N/m}) \times 0.025}{2 \ln \left( 5 \frac{0.577 \times 0.05 + 0.5 \times 0.025}{0.577 \times 0.05 + 2.5 \times 0.025} \right)} = 5.9 \times 10^9 \text{ N/m}$$

### **Lenhoff and McKay**

Lenhoff and McKay also modeled a two-dimensional finite element model to calculate member stiffness. According to their finite element results, they presented a family of curves for each material, which fitted to the second order polynomial equations. The member stiffness of the model in chapter three is calculated according to their equations. The equation is based on the material, which is steel in this study.

$$K_{m,steel} = E \times d \times [0.05385291(l/d)^2 - 0.3933566(l/d) + 1.366381]$$

$$K_{m,steel} = (206.8 \times 10^9 \text{ N/m}) \times 0.025 \times 0.795 = 4.11 \times 10^9 \text{ N/m}$$

## **Wileman and Choudhury**

Wileman and Choudhury conducted finite element analysis of bolted joints having a range of geometries to suggest the dimensionless method of calculating the joint stiffness. The member stiffness for the model, which has been studied in chapter three is calculated as follow

$$K_m = EdAe^{B(d/l)}$$

$$K_m = (206.8 \times 10^9 \text{ N/m}) \times 0.025 \times 0.78715 \times e^{0.62873(0.5)} = 5.57 \times 10^9 \text{ N/m}$$

## **APPENDIX B - Tips for Modeling Bolt in Finite Element Analysis**

In this appendix the steps in modeling joints in finite element study are discussed. Each bolt in a structure has different function that should be analyzed in the simulation. Therefore, before trying to model a bolted connection in finite element packages, we should address the following issues.

- The application of the connection
- Proper element selection
- Bolt characteristics
- Methods of extracting joint stiffness from finite element results.

### **1. The Application of the Connection**

Bolts can be modeled in different ways according to the type of loading, desired accuracy, and simplicity [Montgomery]. Each connection is under a certain type of loading according to figure B.1. Therefore, for modeling the bolted connection that can transfer the load properly, the type of application should be known.

For example, in the connections under tensile and compression load, the head and nut of the bolt should be define as solid. Hence, the load should be able to be transferred through the surfaces between the member and the bolt parts.

In the connections subjected to transverse loading such as joint-lap connections, the bending might have an effect in the bolt shank. Therefore, the contact should also be defined between the bolt shank and the flange, and it is better to model the shank as solid.

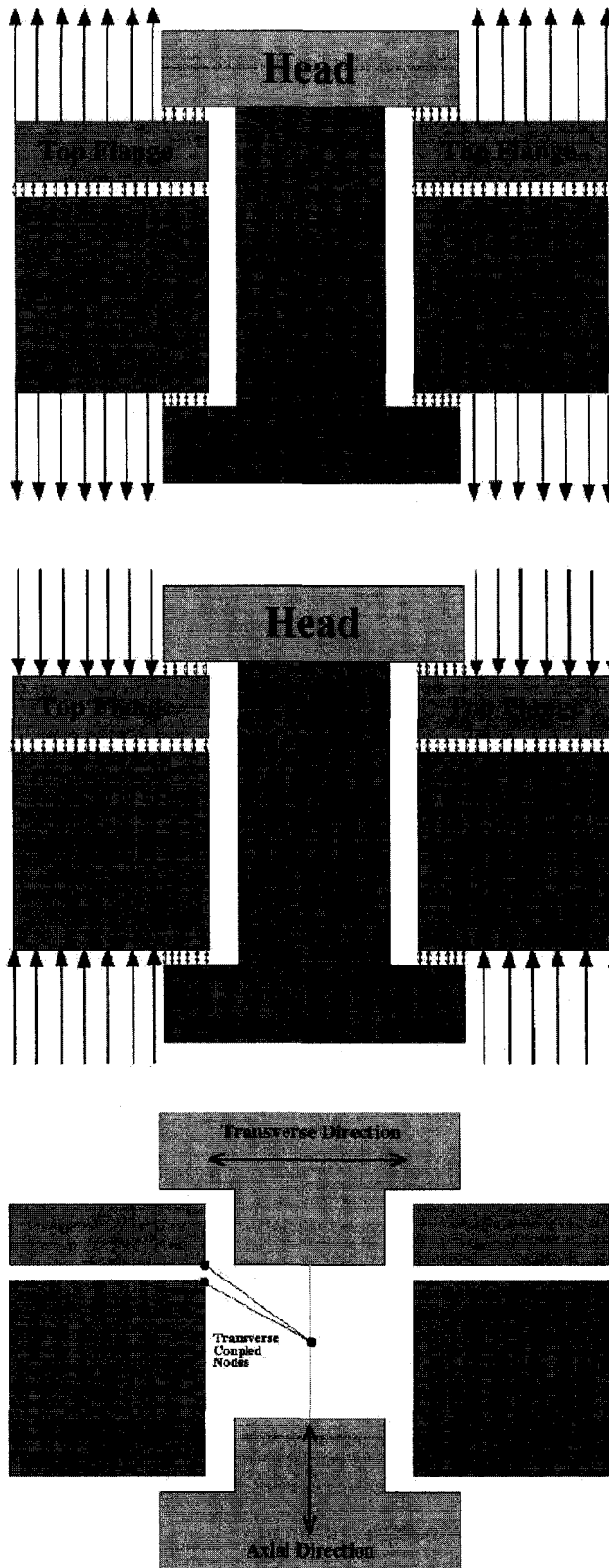


Figure B.1. Bolt under Different Types of Loading [Montgomery]

The *Solid Bolt* modeling is the closest simulation to model the realistic bolt, which is appropriate for investigating all kinds of loading. Most of the researches have used this model to obtain the more accurate simulations.

## 2. Proper Element Selection

The most appropriate element for investigating a bolted connection is the hexahedron elements (Figure B.2). Hexahedron elements have characteristics that can better handle such as plasticity, creep, stress stiffening, large deformation, and large strain all of which might occur in bolted connections.

To choose the proper element, two different issues should be considered. Those are,

- The order of the element; Linear or Quadratic
- The formulation; Full Integration, Reduced Integration, or Incompatible Nodes

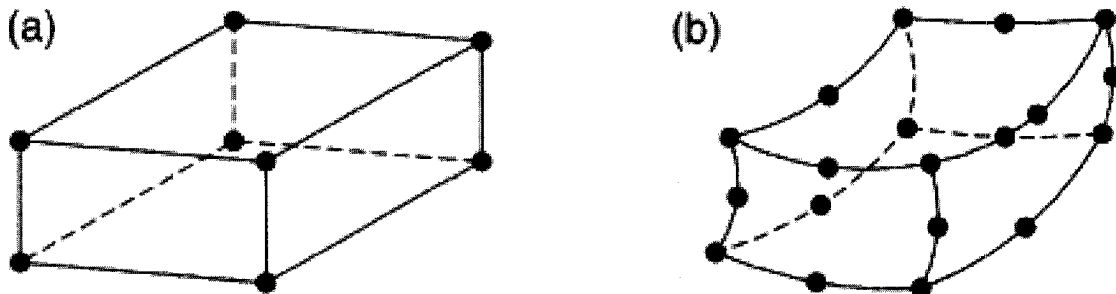


Figure B.2 Hexahedron Element (a) First Order, (b) Second Order [ANSYS (2003)]

In case of elasticity-type (elliptic) problems, much higher solution accuracy per degree of freedom is provided with the higher-order elements.

However, for plasticity-type (hyperbolic) problems, in which elements have to reproduce yield lines, the first-order elements are the most successful type of element [Bursi and Jaspart (1997)].

The first-order element is computationally cheap whereas the second order has better accuracy, and is more appropriate for irregular shapes.

Each element uses a different type of integration for calculating the stiffness matrix. According to the integration method, the element is categorized as full integration or reduced integration.

In reduced integration order, the stiffness matrices are approximated further, but this inaccuracy compensates for the effects of shear locking.

### 3. Modeling bolt characteristics

Preloading and the contact between different surfaces of the bolt are two important characteristics of joints, which should be considered in the analysis. Different methods of applying contact and pretension are explained in this section.

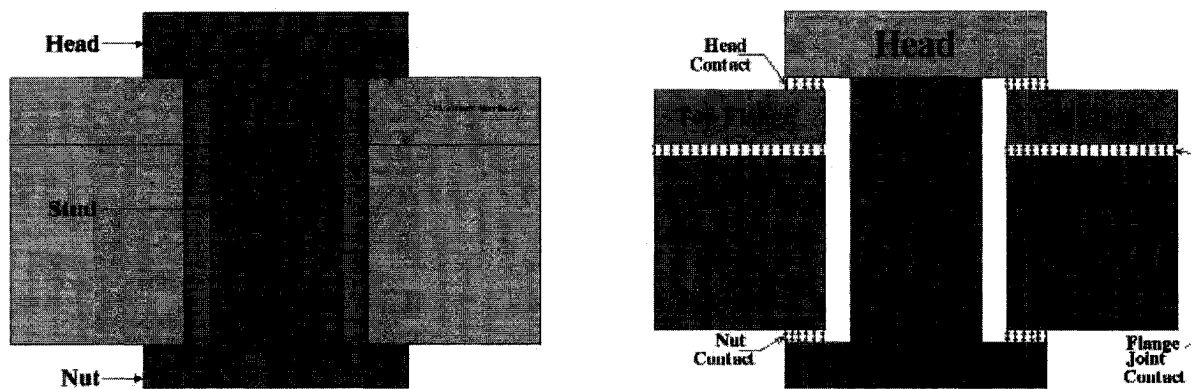


Figure B.3 Different Bolt Characteristics [Montgomery]



## **Contact**

“Contact” in its simplest form can be described by the use of “gap elements” which impose displacement compatibility between user-defined pairs of nodes. However, such elements can only be used when friction can be ignored. In addition, modeling of such elements is a time consuming task. To overcome these problems, commercial finite element packages developed more user-friendly options, such as contact between surfaces and interface elements instead of the node-to-node contact definition required by gap elements.

## **Pretension**

Because of different loading conditions, especially large loads, bolted connections can separate. To minimize this effect, a pretension is applied to the bolt. In finite element studies pretension can be applied in different ways according to the element type or the bolt application.

The pretension modeling can be neglected in some cases that there is no need to represent the exact bolt characteristics [Lim and Nethercot (2004)].

Reid and Hiser (2005) conducted a comprehensive study on modeling the bolted joints with slippage. They used two different techniques for modeling the preload. These two techniques are:

- Using single centrally located discrete spring element
- Using stress based clamping model with deformable elements

In the first technique the spring is defined to act along the axis of the rigid bolt shaft, connecting the head of the bolt to the center of the nut. In order to produce a desired preload, the spring is given an initial offset, which induced an initial force within the spring.

The second technique modeled the pretension more realistically by utilizing deformable solid elements. The desirable realistic preload is produced when the model stretched through an initial deflection.

There are other methods for introducing pretension, which are as follow:

- **Thermal strain or thermal gradient**

Temperature pretension is generated, by assigning the proper material properties to the bolt. The pretension is created by applying thermal strain and thermal gradient or even by creating shrinkage in the bolt stud. From the researchers which have been mentioned through this thesis, Gross and Mitchell (1990), Highlen and Grim (1998), Swanson and Kokan (2002), Allen (2003) and Magi and Goncalves (2004) used this method for their analysis.

- **Initial concentrate load or initial stress/strain**

Initial strain pretension is the more direct approach. In this approach, an initial displacement is applied to the element. Once the solution starts, the initial displacement is considered as a part of the load on the model. The initial strain can be achieved by applying either initial strain itself or having concentrated load or initial stress.

- **Enforced displacement.**

One of the easiest ways to achieve pretension is by applying support displacement to the restrained ends of the bolt shanks. Gerbert and Bastedt (1993) applied the pretension using this method in their study.

- **Applying a shorter length for the bolt**

In this method, the pretension is applied by employing the shorter length than the total thickness of the connecting plates. By considering the shorter length of the bolt, the connection between the bolt head with its respective surfaces, produce the required pretension.

#### **4. Calculating Member Stiffness from Finite Element Results**

There are different ways of calculating the member stiffness from finite element results according to the method of preload. When a concentrated load is applying to represent the pretension, member stiffness will be calculated, by dividing the applied load over the average deflection of the member according to equation 1.

$$Stiffness = \frac{Applied\ Load}{Average\ Member\ Deflection} \quad (1)$$

The other method of preload is to enforce a uniform deflection at the bolt head to member interface effectively. Therefore, the stiffness will be calculated according to equation (2).

$$Stiffness = \frac{Applied\ Load}{Enforced\ Deflection} \quad (2)$$

The strain energy method is another procedure for calculating bolted joint stiffness with the finite element method. This method is simple and eliminates the need to calculate average deflection results at the bolt head to the member interface.

A derivation of bolted and member stiffness formulas are based on the magnitude of induced preload. The formulas were derived by treating the bolt and member as two springs connected in parallel [Allen (2003)]. By calculating the bolt and the member

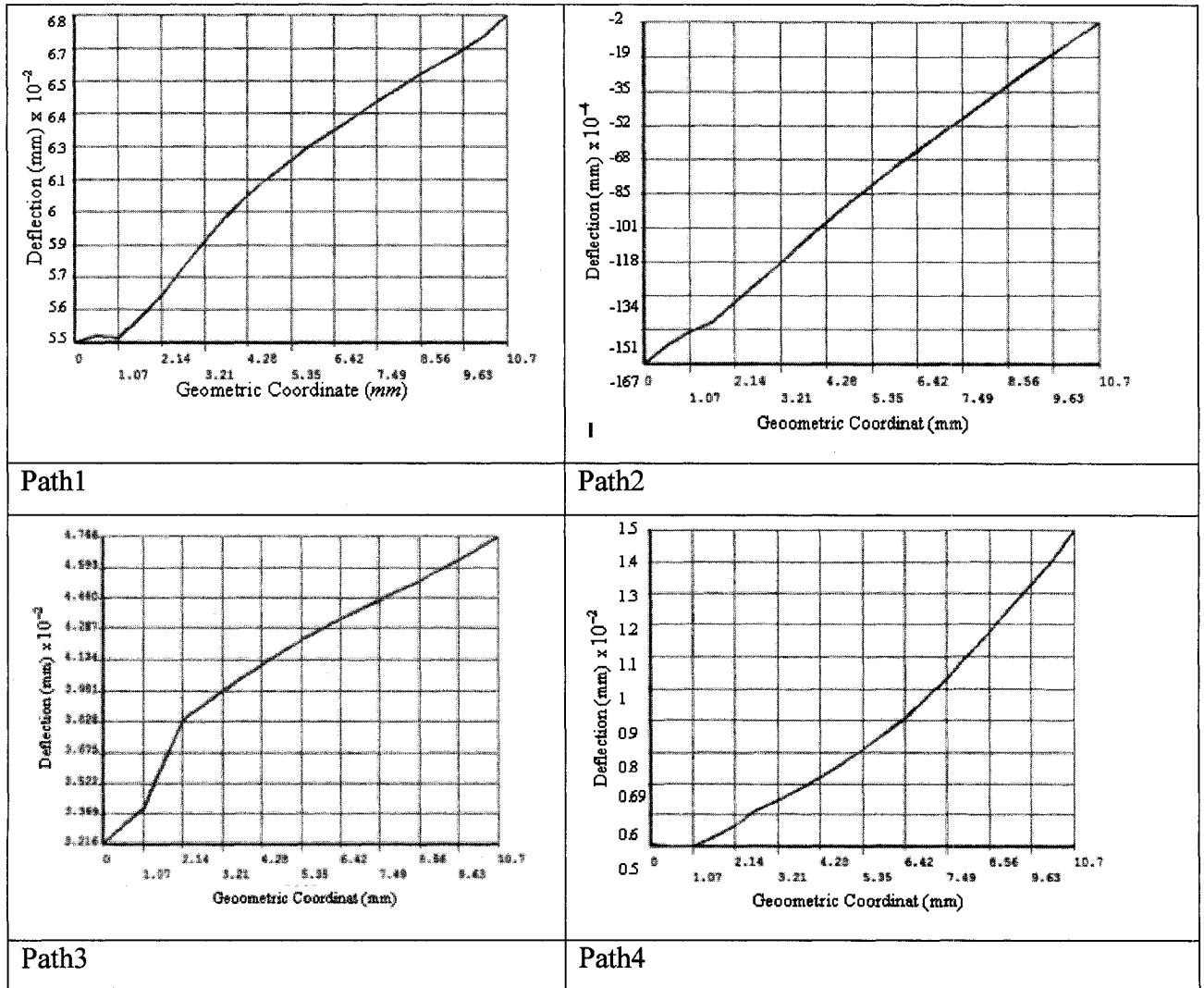
strain energies, and substituting the values in the following equations, the member and bolt stiffnesses can be easily calculated.

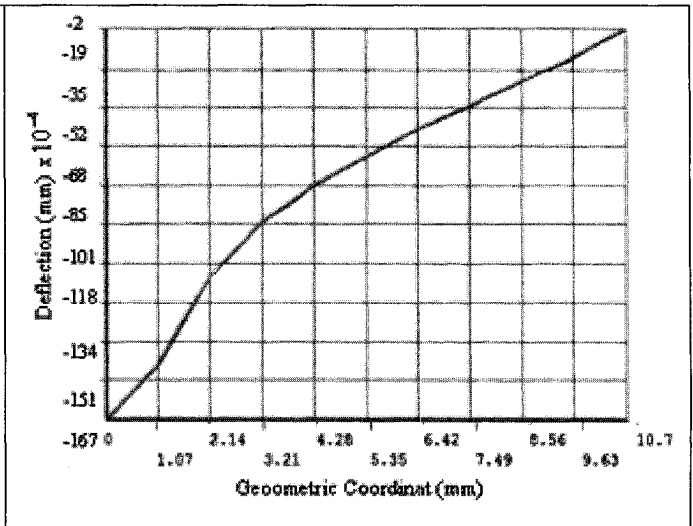
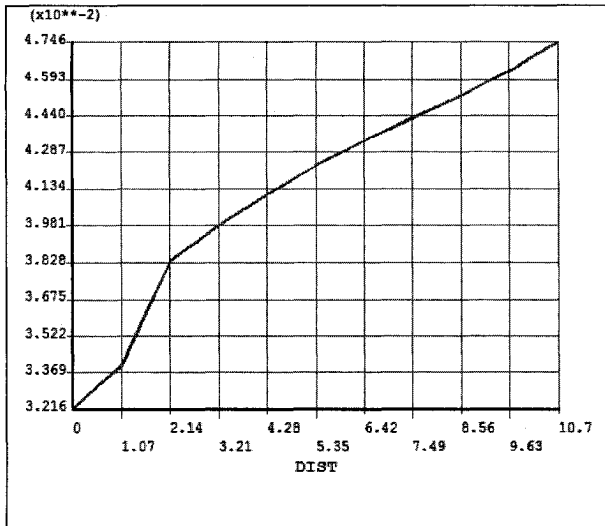
$$k_m = \frac{-P_i}{\alpha_b \Delta T_b L_b} \left( 1 + \frac{U_b}{U_m} \right) \quad (3)$$

$$k_b = \frac{-P_i}{\alpha_b \Delta T_b L_b} \left( 1 + \frac{U_m}{U_b} \right) \quad (4)$$

## APPENDIX C: Displacement of the Member Depicted on Nine Paths

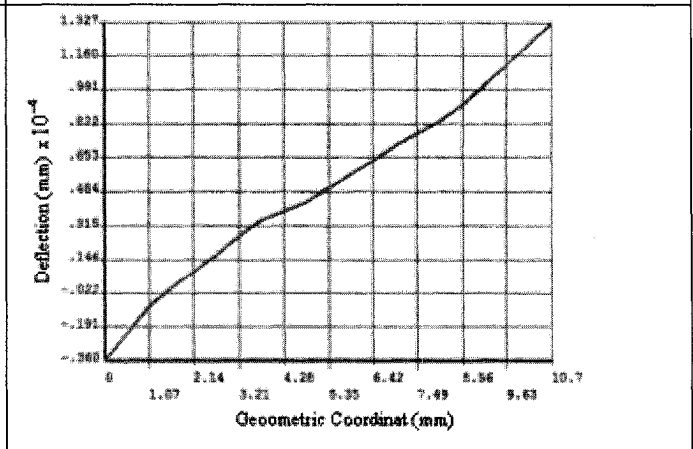
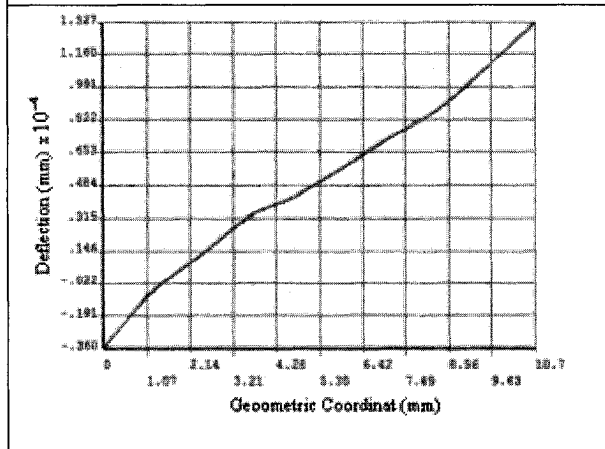
To read the displacement values, which are needed for calculating Zhang's model, nine different paths are defined. The displacement in z direction is mapped into these paths. The first four paths plotted are the  $U_z$  on the centerline of the bolt head, and the next four paths  $U_z$  are on the bolt hole interface. Path 9 displays the displacements at the center of the bolt shank. The displacements are mapped into these paths before and after the separation. The plotted paths for the after separation condition are given in this appendix as an example. The vertical axis is the displacement and the horizontal axis is the geometric coordinate of the paths. Units are all millimeter.





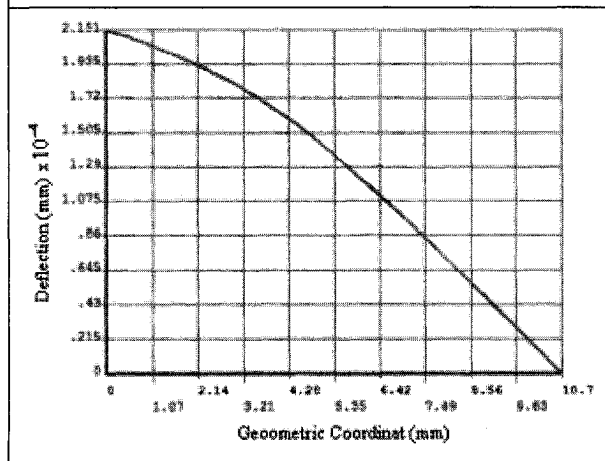
Path5

Path6



Path7

Path8



Path9

Figure C.1 Displacement of the Member Depicted on Nine Different Paths

## VITA AUCTORIS

NAME	Negar Rasti
PLAVE OF BIRTH	Tehran, Iran
YEAR OF BIRTH	1979
EDUCATION	Narjes High School, Tehran, 1993-1997 University of Guilan, Rasht, Iran 1997 - 2001. B.Sc. University of Windsor, Windsor, Ontario 2004 - 2007. M.Sc.